Real-time monitoring the electrical properties of pastes to map the hydration induced microstructure change in cement-based materials

Cement and Concrete Composites 132 (2022) 104639

Contents lists available at ScienceDirect

Cement and Concrete Composites

journal homepage: www.elsevier.com/locate/cemconcomp

Real-time monitoring the electrical properties of pastes to map the hydration induced microstructure change in cement-based materials

Liming Huang [a,b,*], Luping Tang [a], Ingemar Löfgren [a,c], Nilla Olsson [d], Zhenghong Yang [b]

[a] Department of Architecture and Civil Engineering, Chalmers University of Technology, 41296, Gothenburg, Sweden
[b] Key Laboratory of Advanced Civil Engineering Materials Ministry of Education, Tongji University, Shanghai, 201804, PR China
[c] Thomas Concrete Group AB, Södra Vägen 28, 41707, Gothenburg, Sweden
[d] NCC Building, Division Building Sweden, 17080, Solna, Sweden

ARTICLE INFO

Keywords:
Electrical conductivity
SCMs
Formation factor
Setting
Percolation theory
Chloride migration

ABSTRACT

The effect of the supplementary materials (SCMs) on the moisture content and ion diffusivity at different hydration time is important for the service life modelling of modern concrete. This study designed a simple but valid method to monitor the microstructure change in pastes during hydration. A procedure easy to implement was proposed to detect the water content in pastes. The electrical conductivity of pore solution was evaluated by the evaporable water content in pastes and chemical composition in the binders. Results show that the electrical properties of pastes (conductivity, formation factor and its growth rate) can effectively indicate the hydration reactivity of binder, pore connectivity and volume of pore solution in the hardened pastes. The effect of water-binder ratio and SCMs on the structure of pastes are effectively indexed by the formation factor which is the conductivity of pore solution divided by that of paste. The inflection point of average growth rate of formation factor is a good index for the final setting of pastes. The relation between volume of evaporable water and formation factor is well demonstrated by the extended percolation theory. The real-time monitored electrical conductivity and formation factor of pastes can be used to calculate the chloride migration coefficient in hardened cement pastes.

1. Introduction

The moisture content and ion diffusivity in the cement-based materials change with the curing time due to the continuous hydration of binders. The hydration of binders is a complex process involving the dissolution of reactants and precipitation of products. The initial nucleation and growth of hydration products at the solid-liquid interface leads to the formation of clusters that eventually connect into an elastic network structure, resulting in the setting of paste due to the percolation of connection [1]. As hydration reaction continuously proceeds, the growth of products modifies the structure of the hardened cement-based materials. Because the desirable engineering characteristics of hardened concrete (strength, dimensional stability, and durability) depend on the microstructural features (i.e., the type, amount, and distribution of solids and voids) [2], a lot of models were proposed to simulate the microstructure development during hydration [3]. Despite of having some progresses, we are far away from reaching a complete simulation that allows engineers to perform a precise prediction on the performance of concrete. To better understand the hydration process and provide data for simulation, a reliable in-situ test of hydration and microstructure development of concrete is of great significance. The use of supplementary cementitious materials (SCMs) are currently recognized as the main way to produce sustainable concrete [4,5]. Therefore, the anticipated mechanical performance and durability of modern concrete require a good knowledge about the hydration and microstructure evolution of both ordinary Portland cement (OPC) and the blended pastes.

There are many well-used methods to measure hydration rate and degree of cementitious materials, such as calorimetry, chemical shrinkage, chemically bonded water, X-ray diffraction and scanning electron microscope [6,7]. For the microstructure analysis, Monteiro et al. [8] had a detailed review to summarize the most advanced methods used in the research of cement-based materials. However, only a few of those methods can be applied as an in-situ measurement without any special treatment of samples. Moreover, the allowed dimension of samples is limited for the measurement by those methods.

* Corresponding author. Department of Architecture and Civil Engineering, Chalmers University of Technology, 41296, Gothenburg, Sweden.
E-mail address: limingh@chalmers.se (L. Huang).

https://doi.org/10.1016/j.cemconcomp.2022.104639
Received 22 January 2022; Received in revised form 18 April 2022; Accepted 16 June 2022
Available online 21 June 2022

Low field proton NMR is a promising way to monitor the hydration [9] and structure evolution [10] of paste. However, the relaxation signals will be affected by paramagnetic matter (such as Fe) [11], so it is not a compatible method for the investigation of grey cement and the blended pastes.

Apart from all the above methods, the test of electrical conductivity was used in many previous studies [12–16] as a qualitive way to indicate the hydration and structure of the cement-based materials. The conductivity/resistivity of concrete was used as a viable index to study hydration and a good approach for designing the automated monitoring system in construction [17]. Karmazsin and Murat [18] designed an apparatus for a simultaneous test of the isothermal calorimetry and electrical resistance. Their results showed that the evolution of resistance was highly comparable with the calorimetry evolution during the hydration of calcium sulfate hemihydrate in a small cell. A similar setup was used to study the influence of chemical admixtures on the hydration of OPC [19], and the authors found that the increase in the electrical conductivity are in the same order as that in the heat liberation rate. Singh et al. [20] used conductivity test, combined with heat release and other analysis methods, to reveal the effect of citric acid on the hydration of OPC. They concluded that the ionic mobility and concentration of charge carriers were decreased by citric acid so that the hydration of cement was altered. The measurement of electrical conductivity was also frequently applied in the investigation of the blended system. Abo EI-Enein et al. [21] proposed several empirical equations to describe the correlations between water-binder ratio (w/b) or silica fume content and electrical conductivity. A similar empirical equation was correlated between conductivity of paste and kaolinite content [22]. The hydration of granulated slag blended with cement kiln dust or silica fume [23], and the rheological properties of pastes blended with silica fume were connected to the conductivity evolution with time [24]. Chrisp et al. [25] applied an auto-ranging impedance analyzer to test the conductivity of cover zone concrete blended with slag and fly ash. They used a normalized conductivity to indicate the effect of wetting and drying. McCarter [26] et al. used the same setup for monitoring the electrical response of alkali activated paste before 48 h and the conductivity of hardened concrete exposed at the marine environment. The normalized conductivity based on the value at the initial time was defined to indicate the hydration of concrete with different binder types and w/b [27]. The evolution of conductivity was classified into four stages with respect to the dissolution and precipitation during the early hydration. However, some analysis of conductivity change based on pore solution concentration in Ref. [27] is contradictory to the tested ion concentration in pore solution in some published papers [28,29].

It is a challenging but meaningful work to find a quantitative relationship between the conductivity and hydration or other properties of cement-base materials. Conduction of electric current in cement paste includes two path ways: one is ionic conductivity through pore solution, which depends upon the temperature [15,30–32], type of ions and its concentration [33,34], and the connectivity between the high conductive solution; the other is electronic conduction through the gel-water and unreacted cement particles, particularly compounds of iron, aluminum and calcium [35]. By taking these factors into account, some empirical relations were proposed to correlate the conductivity with hydration time, porosity, hydration degree [36], mechanical performance (compressive strength [37,38]) and diffusivity [39,40]. Wilson et al. [41] found a general correlation between the effective chloride migration coefficient from their method and the bulk conductivity of pastes, but the white cement pastes deviated from the general line when the coefficient was correlated with inverse of formation factor or pore connectivity. Chidiac and Shafikhani [42] developed model based on the measured conductivity of concrete and the calculated conductivity of pore solution. Their model is effective in estimating the chloride migration coefficient in both OPC and the blended concrete.

The change of electrical conductivity of paste during hydration will be determined by the evolution of intrinsic factor as shown in Fig. 1. Hydration of minerals induces a change of phase assemblage and internal moisture, which in the meantime forms the structure of paste. As now popularly acknowledged [43], the availability of moisture and pore distribution in paste will, in turn, makes impact on the later age hydration. The volume and ionic concentration of pore solution was related to the phase assemblage and moisture content through thermodynamic laws. Besides the composition of paste, the connectivity of pore solution (similarly, pore connectivity) is the other factor that controls

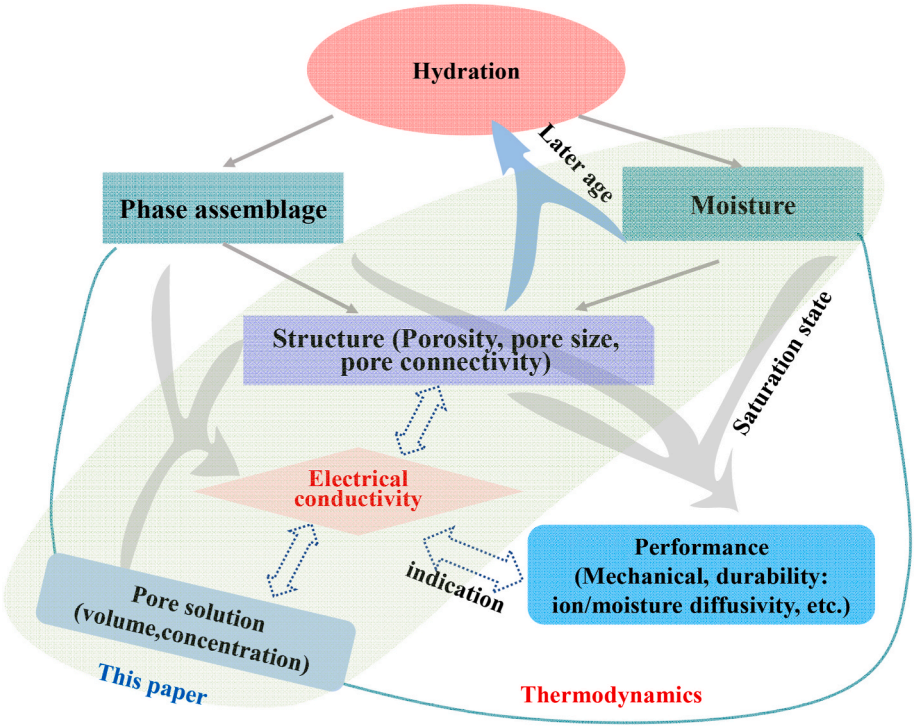

Fig. 1. The logical relationships between the electrical conductivity, hydration, and performance of paste.

the electrical conductivity in pastes. The mechanical performance and durability of cement-based materials are determined by its phase assemblage, microstructure, and the saturation state. These properties for one specific proportion can be qualitatively or empirically indicated by the conductivity, but it lacks a general description in both OPC and the blended pastes. A generally quantitative relationship is of great significance for not only the scientific research but also industrial application.

This paper presents an investigation on discovering how the electrical properties correlate with the hydration process, structure evolution and chloride migration in both OPC and the blended pastes. We designed a simple setup for an instantaneous conductivity monitoring, and then mainly focused on the deep understanding of the relationship between the conduction and structure of paste. A novel procedure was developed to detect the evaporable water content of paste so that the electrical conductivity of pore solution was calculated based on chemical composition of binder and volume of evaporable water. The formation factor was calculated to distinguish the effect of pore solution and structure on the conduction. Its growth rate was defined to indicate the setting and hydration reactivity of pastes. The electrical properties measured by the invented method were also correlated to the chloride migration coefficient. A good correlation has been found between formation factor and moisture content based on an extended percolation theory [44].

2. Experiments

2.1. Materials

The used cement is an ordinary Portland cement CEM I 52.5 R with a Blaine surface of 525 m^2/kg. Three kinds of SCMs were considered, including slag Bremen (SL) with a Blaine surface of 420 m^2/kg from Thomas cement AB, Fly ash (FA) from Cementa, and limestone from Nordkalk with a D_{50} = 18 μm (LL). The chemical composition of each binder is shown in Table 1. The limestone has a calcite content ~89% and a relatively high SiO_2. Table 2 presents the mix design of 11 samples. In the binary systems, the replacement content of cement with SL and FA is the same as 35% by weight. In the ternary system, OPC was replaced with 35% SL and 16% LL. Pastes were mixed with three different *w/b* with 0.35, 0.45 and 0.55 respectively, except for the FA blended pastes with two ratios (0.35 and 0.45).

2.2. Procedures and methods

2.2.1. The electrical conductivity test

The electrical conductivity of paste was measured by a four-electrode method to minimize the effect from polarization. The electrodes were positioned in the Wenner configuration referring to Ref. [46] as shown in Fig. 2. The stainless screws were used as the electrodes and these are positioned in the middle line with a parallel distance of 25 mm to the bottom line, and the space between electrodes is 40 mm. A brief circuit diagram of the setup is presented in right of Fig. 2. The whole system was recorded and controlled by a datalogger. We used two relays (a and b) to control the power supply and one relay (c) to control the data collection. Besides during the time for instant test, the paired electrodes were connected to avoid polarization difference. The electrical conductivity of the samples was calculated as a semi-infinite slab with the voltage and current value. The whole setup was calibrated with the standard conductive solution (KCl) in the range of 0.015–74.97 mS/cm. In the first 24 h, the datalogger released an instant signal every 2 min to connect power system to provide a constant current (0.5–1 mA). Simultaneously, relay c created the connection for collecting the voltage between the two electrodes in the middle. It takes about 0.2 s to finish one instant test. The time interval was switched to 10 min from 1 day to 12 days. The data after long-term hydration was further collected at 28, 90 and 180 days.

The dry binder was homogenously mixed in a ceramic rotator with balls (D = 20–25 mm) at 12–20 rpm for 10 h. Firstly, water with 35% weight of binder was added into binder and then it was mixed with a slow rate by the planetary mixing machine for 60 s. Secondly, the rest of water was added up to the target *w/b* before a high rate stirring for 120 s. Afterwards, the pastes were poured into the small plastic boxes with four electrodes and a volume capacity of 1000 mL. The sample was sealed with the cap and put in the curing room with a constant temperature of 20 ± 1 °C. The data collection started at about 10 min after water addition.

2.2.2. Water distribution test

An easily implementing procedure was designed for the determination of water content in pastes (see Fig. 3). The pastes were mixed with the same procedure in section 2.2.1. Samples were casted in a Petri dish

Table 2
The mix proportion of samples (LOI_b: the normalized loss of ignition of binder system).

Samples	Binder	w/b	LOI_b
P035	OPC (SH P Slite CEM I 52.5 R)	0.35	2.5%
P045	OPC (SH P Slite CEM I 52.5 R)	0.45	
P055	OPC (SH P Slite CEM I 52.5 R)	0.55	
P135	65%OPC+35%FA	0.35	2.85%
P145	65%OPC+35%FA	0.45	
P235	65%OPC+35%SL	0.35	1.2%
P245	65%OPC+35%SL	0.45	
P255	65%OPC+35%SL	0.55	
P335	49%OPC+35%SL+16%LL	0.35	0.85%
P345	49%OPC+35%SL+16%LL	0.45	
P355	49%OPC+35%SL+16%LL	0.55	

Table 1
Chemical composition of different binders (*LOI*: loss of ignition; δ_i: mole of chemical composition per gram binder).

Chemical Composition	CEM I 52.5 R		Slag		Fly ash		Limestone
	wt%	δ_i(mol/g)	wt%	δ_i(mol/g)	wt%	δ_i(mol/g)	wt%
CaO	62.2	1.11E-02	39.11	6.98E-03	5.1	9.11E-04	49.5
SiO_2	19.6	3.06E-03	36.63	5.72E-03	54.6	8.53E-03	9.0
Al_2O_3	4.5	4.41E-04	13.56	1.33E-03	22.4	2.20E-03	0.6
Fe_2O_3	3	1.88E-04	0.49	3.06E-05	8.7	5.44E-04	0.3
SO_3	3.5	4.38E-04	0.27	3.38E-05	0.8	1.00E-04	0.03
MgO	3.5	8.75E-04	8.52	2.13E-03	1.8	4.50E-04	–
K_2O	1.01	1.07E-04	0.57	6.06E-05	2.1	2.23E-04	0.3
Na_2O	0.27	4.35E-05	0.42	6.77E-05	1	1.61E-04	0.1
Cl	0.07	1.97E-05	0.009	2.54E-06	–	–	–
Sulfide	–	–	0.73 ×	–	–	–	
LOI	2.5		−1.07		3.5		40.1

× Note: The sulfide in slag will be oxidized during the LOI test, so this induces an increase of weight. Although the hydration also makes oxidization of sulfide [45], we assume that its oxidization is rare due to the low hydration degree at early age.

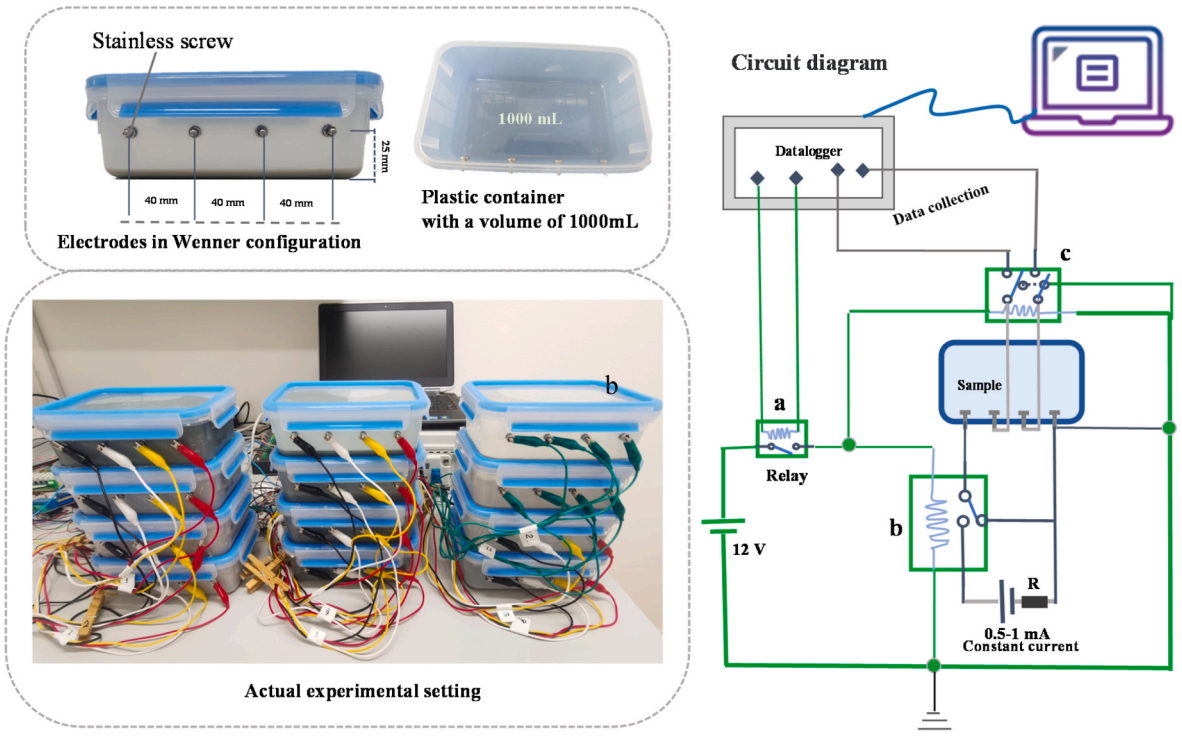

Fig. 2. A simple setup for monitoring the conductivity during hydration.

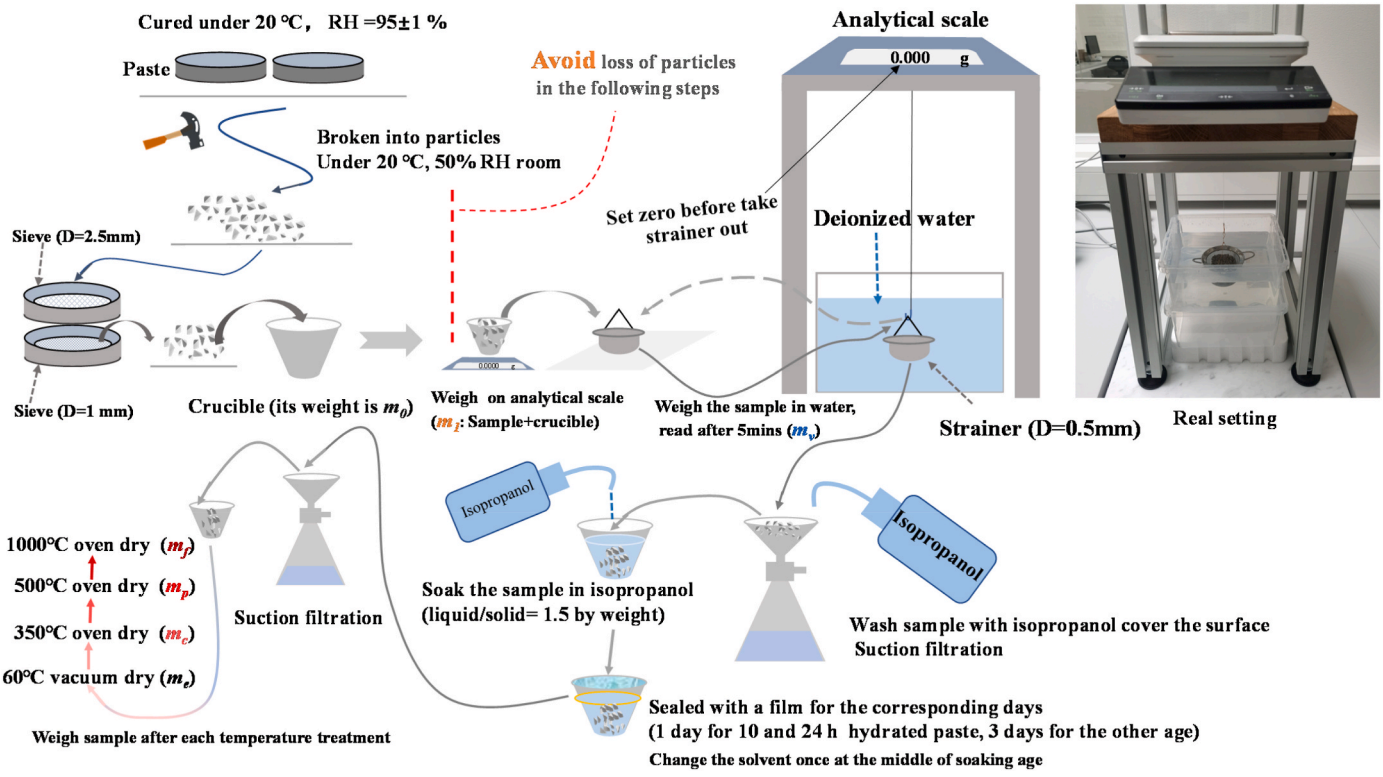

Fig. 3. The procedure for testing the water distribution in paste.

and cured in a box with 97 ± 1% RH at 20 °C. The hardened pastes were broken into pieces after a series of curing times. Particles with size in a selective range (D = 1–2.5 mm) were collected for the treatment in the next step. To ensure the validity of data, the weight of particles should be ≥ 10 g, and the accuracy of analytical balance is at least 0.001 g. The mass of dry empty crucible was weighed and recorded as m_0. The crucible containing particles was weighed and recorded as m_1 and then particles were transferred into a small strainer (D = 0.05 mm). The mass of particles immersed in water was weighed by the analytical balance that was zero set with holding of the strainer. Thereafter, the particles

were washed with isopropanol (IPA) before transferring back to the crucible. Samples were immersed with IPA with a liquid/solid ratio of 1.5 and sealed with a cling film. The procedure was finished within 30 min from water addition to the sealing. IPA exchange method is recommended as the preferred way for stopping the hydration and drying the paste [6]. Zhang and Scherer [50] asserted that the exchange duration need to be sufficient to reach ~99% IPA at the sample center. This exchange degree can be reached after 5-h immersing for sample with size of 1 mm. For a complete exchange of evaporable water, the immersing duration is at least 24 h for samples in this study (see Fig. 3). We changed the solvent once at the middle immersing age.

Samples were filtered, moved back to the crucible, and followed with a vacuum drying at 60 °C (V60) for 24 h. The mass of vacuum dried crucible with sample was weighed (m_e). Afterwards, the crucible was immediately put into a furnace with a temperature pre-heated to 105 °C. It was heated up to 350 °C with a rate of 5 °C/min and this temperature was maintained as constant for 2 h. After it was cooled down to 105 °C, it was moved out with the heat-resistant gloves and weighed on the analytical scale with an insulation layer between crucible and scale. The same step was repeated for the other temperatures, starting again at 105 °C to the target temperature (500 and 1000 °C, respectively) with a holding time of 2 h. The weight of crucible with sample at V60, 350, 500 and 1000 °C was recorded as m_c, m_p and m_f, respectively.

2.2.3. Setting time test

The setting of pastes was tested by a Vicat needle according to ASTM C191-08 under an environment temperature of 20 °C and relative humidity of 50%, except that pastes were mixed with the w/b of 0.35, 0.45 and 0.55 instead of w/b a for normal consistency. The fresh pastes were kept in a moist box with RH of 97% between the Vicat needle measurement intervals.

2.2.4. Chloride migration test

Pastes were casted into a rubber cylinder mould ($\Phi_{in} = 50$ mm, $h =$ 110 mm). After a sealed curing for 1 day, specimens were demoulded and moist cured until the age of 28, 90 and 180 days, respectively. Two samples with a thickness of 50 mm were cut from each specimen for the RCM test at the specified age. The test was performed according to NT BUILD 492 but without the vacuum saturation procedure because the specimens were moist cured before the test.

2.3. Determination of the evaporable and bound water content

With the weight from section 2.2.2, we can calculate the weight loss percent at the corresponding temperature ranges, so the evaporable water (Epw) percent with respect to binder (φ_{epw}) is stated as:

$$\varphi_{epw} = \frac{m_1 - m_e}{m_{ub}} \tag{1}$$

where m_{ub} is the mass of the mixed binder. Given that the carbonation of samples during early age can be neglected, the m_{ub} for paste without LL can be calculated by Eq. (2).

$$m_{ub} = \left(m_f - m_0\right)/\left(1 - LOI_b\right) \tag{2}$$

The weight loss at the temperature range of V60~350 °C, 350~500 °C and 500~1000 °C can be calculated by Eqs. (3)–(5), respectively.

$$\varphi_{\sim 350} = \frac{m_e - m_c}{m_{ub}} \tag{3}$$

$$\varphi_{350\sim 500} = \frac{m_c - m_p}{m_{ub}} \tag{4}$$

$$\varphi_{500\sim 1000} = \frac{m_p - m_f}{m_{ub}} - LOI_b \tag{5}$$

The CO_2 release from LL within the temperature range of 500~1000 °C needs to be subtracted for LL blended paste. Hence, the actual weight of binder is $m_{ub}{}'$ by Eq. (6).

$$m_{ub}{}' = \left(m_f - m_0\right)/\left(1 - 44\% \times P_{lm} - LOI_b\right) \tag{6}$$

where P_{lm} is the replacement percentage of LL and this is 16% in this study. In addition, the weight loss from moisture between 500 and 1000 °C for LL blended is:

$$\varphi_{500\sim 1000} = \frac{m_p - m_f}{m_{ub}{}'} - 44\% \times P_{lm} - LOI_b \tag{7}$$

Theoretically, according to the law of conservation of mass, we can get the mass balance Eq. (8). This can be used to check the accuracy of the test procedure.

$$\varphi_{epw} + \varphi_{\sim 350} + \varphi_{350\sim 500} + \varphi_{500\sim 1000} \equiv w/b \tag{8}$$

3. Results

3.1. Real-time conductivity of pastes with different w/b

The real-time monitored electrical conductivity of pastes is shown in Fig. 4. The evolution of electrical conductivity up to 400 days was classified into four regions by McCarter et al. [27] and the author had a detailed discussion on the relationship between the hydration process and conductivity evolution. Herein, some different explanations for the change of conductivity will be specified. Exemplifying with OPC paste with $w/b = 0.35$, The evolution of conductivity can be classified into four stages before 14 h (Fig. 4a).

The great increase of conductivity in stage I was not mentioned in Ref. [27]. This results from the fast increase in concentration of OH^-, K^+ or Na^+ in pore solution mainly due to the quick dissolution of alkali metal ions after water addition. Samples with w/b of 0.45 have the highest conductivity in OPC pastes. The increase in w/b dilutes the K^+ and Na^+concentration in pore solution, so P045 has a higher conductivity than P055. For the paste with w/b of 0.35, the connectivity of pore solution is the lowest. Although P035 has a higher alkali concentration, compared to P045, the electrical conductivity is lower. The blending of SCMs reduces the alkali concentration in the pore solution to decrease the initial conductivity. Lothenbach and Scrivener [47] ascribed the reduction in alkali concentration to three effects: dilution of OPC; consumption of portlandite leading to lower Ca concentration; increase of alkali uptake in C-A-S-H. The reduction effect only comes from the dilution effect since few products precipitate at early ages.

Stage II corresponds to the induction period. The concentration of Si ions increases during this period, but it has little influence on the conductivity. The concentration of Ca in this period is constant and even has a little reduction [28,48]. The slow growth of conductivity is due to the slow increase in pH and concentration of alkali ions to reach a critical supersaturation state of reactants. The w/b has few effects on the duration of this period, which is consistent with its effect on the heat release rate at this period [49]. At the end of this stage, the early hydration products (ettringite, C–S–H and portlandite) connects into a net structure for initial setting and results in the occurrence of stage III. The blending of FA, SL and LL prolongs the time from stage II to III. Because the reactivity of these SCMs is lower than cement, it takes more time to build the sufficient connections between particles.

Although the main conductive ions (OH^-, Na^+ and K^+) have an increase during stage III [28,48], the conductivity of paste reduces due to the structure growth. The increase in w/b induces a longer stage III and this effect is more significant on blended system than OPC. The rapid growth of hydration products brings about the stage IV. The further fast growth of hydration products leads to the fill and blocking of pores in structure. Meanwhile, the consumption of free water reduces the volume of pore solution. These dual effects lead to a dramatic decrease in

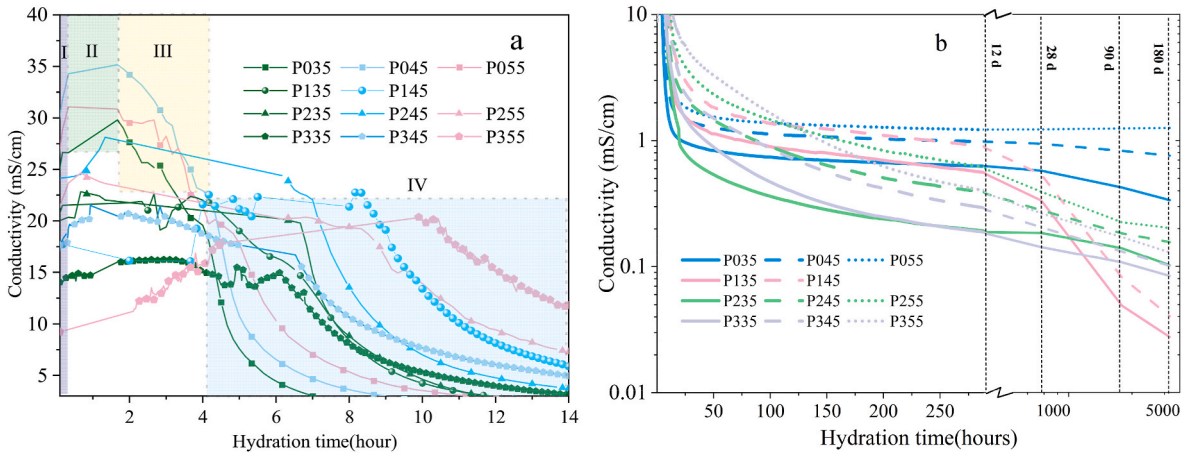

Fig. 4. Electrical conductivity of pastes during hydration: (a) detailed data before 14 h; (b) the measured data up to 180 days.

conductivity. The increase in *w/b* seems to have few effects on the decreasing rate of conductivity, but SCMs have impact on that rate. Fig. 4b shows that the conductivity of OPC paste falls into a rather stable stage with a very low decreasing rate. The conductivity of FA blended paste has the similar trend with a little higher decreasing rate at the stable stage compared with OPC from 10 h to 12 days. However, it has the most evident decrease from 12 to 180 days due to the pozzolanic hydration of FA. The conductivity of SL blended has a continuous decease up to 180 days because of its high latent hydraulic reactivity. This trend was also found in many previous works [27,50,51], which confirmed again that the conduction test is an effective way to indicate the reactivity of SCMs.

3.2. Water distribution and hydration degree of pastes

Fig. 5a presents the weight loss of all pastes in different temperature ranges. According to Refs. [52,53], the solvent exchange by IPA starts with the replacement of the pore water, and then the water in small pores (interhydrate and interlayer) moves out under the concentration gradient. Therefore, the weight loss from vacuum dried at 60 °C includes not only the free water in pore solution but also the interlayer water, which is here classified as evaporable water (Epw). A clear tendency can be observed for all pastes, that is, a higher *w/b* results in a higher content of Epw at any hydration ages. The bound water or nonevaporable water (Nw) denotes the weight loss after the vacuum dried to oven dried at 1000 °C. It should be noted that, apart from dehydrolysis, the decarbonation [6,7,54] and LOI will induce a weight loss between 500 and 1000 °C. The LOI was subtracted in Eqs. (1)–(7). For the pastes with *w/b*

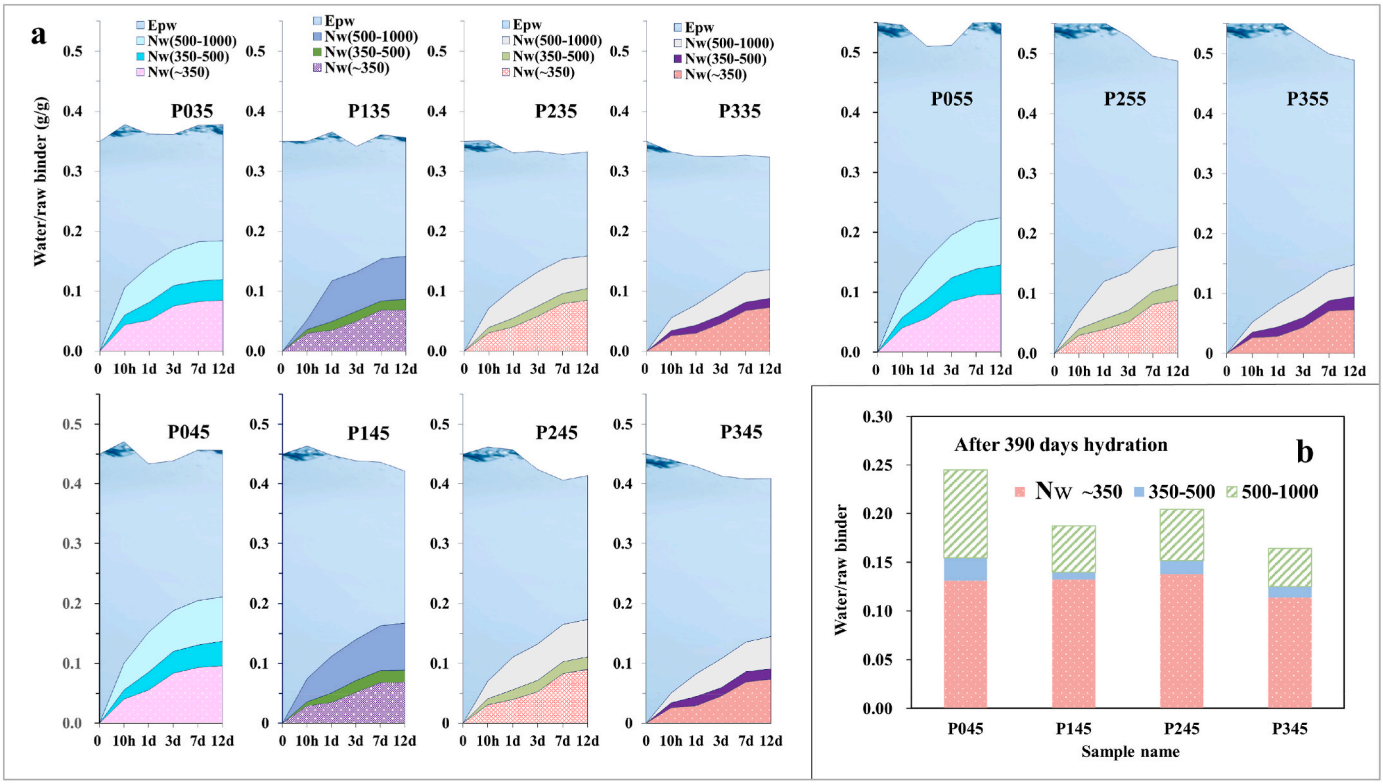

Fig. 5. Water distribution in pastes at different hydration times.

at 0.35 and 0.45, the ratio of final total water to raw binder in Fig. 5a is close to the *w/b*, so it implies that the carbonation is very weak.

OPC paste with *w/b* = 0.35 shows a slow growth in weight loss between V60 and 500 °C from 3 to 12 days. An increase of *w/b* to 0.45 and 0.55 augments the Nw of pastes after 1 day at all ranges, which confirms that the water availability is critical for the later age hydration. Nw of FA blended paste keeps rather stable after 7 days. FA blended pastes has a lower weight loss than OPC between V60 and 500 °C because a lower amount of OPC in binder generates less early-precipitated products (gypsum, ettringite, C–S–H, brucite and portlandite etc. [6,55]) whose dehydrolysis occurs up to 500 °C [6]. The blending of SCMs will accelerate the hydration of clinker [56], so Nw of FA pastes between 500 and 1000 °C is not even lower than OPC paste. According to the general results [7], The bound water (V60–950 °C) normalized to OPC increases with the increase in content of FA [57], so FA not only increases the hydration of OPC but also contributes to bound water in pastes by itself. A similar effect is observed in our results especially for water loss between 500 and 1000 °C. The *w/b* has a weaker effect on the bound water of FA blended than that of OPC paste.

The bound water of SL pastes between V60 and 500 is lower than that of OPC. Similarly, an enhancement effect on bound can be observed if we normalized the bound water to OPC content and this is consistent with Escalante-Garcia's investigation [58]. The weight loss of the SL blended paste is close to that of FA pastes with the same *w/b* between V60 and 1000 °C, but SL pastes have a higher content of Nw than FA pastes between V60 and 500 from 7 to 12 days. The ternary system with LL has the similar trend in the development of bound water as SL binary pastes. The main influence is that the replacement of LL induces a higher content of Epw than the other binder system.

It is controversial to use the weight loss up to 1000 °C as an index for the hydration degree of cement because it includes the loss of CO_2 and LOI. Nathan and Narayanan [59] proposed a model to distinguish the enhancing effect from SCMs, but they did not take the decarbonation into account. In the R3 method developed by François Avet et al. [60], a good correlation was found between bound water at 110–400 °C and cumulative heat release from calcined clay blended pastes. The authors chose 400 °C as the upper temperature based on the initial decomposition of portlandite. However, the lowest decomposition temperature of

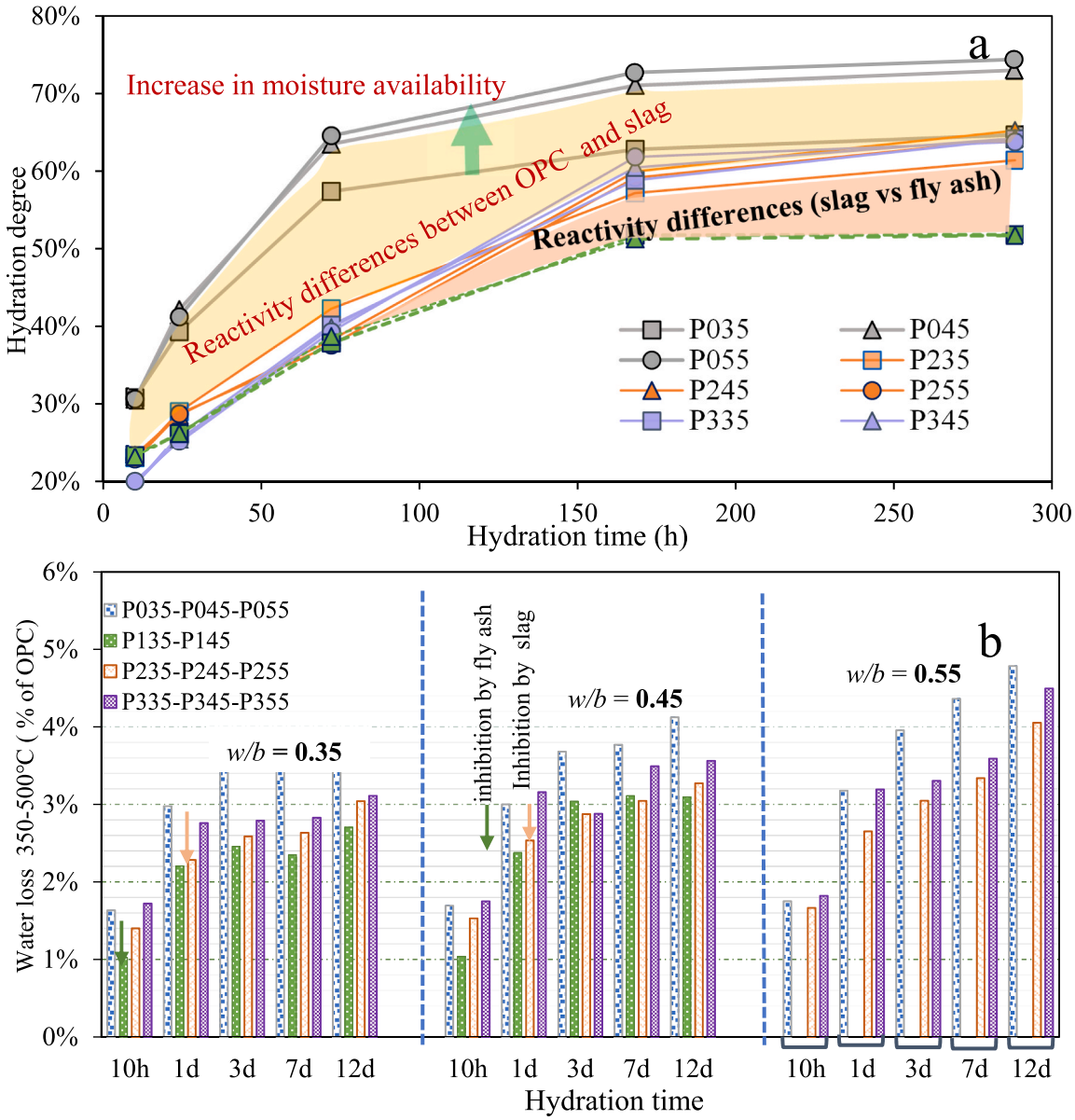

Fig. 6. Hydration degree (a) and the normalized water loss between 350 and 500 °C (dehydrolysis of portlandite) (b) at different hydration times.

portlandite is about 350 °C [61]. Therefore, we used the weight loss between V60 and 350 °C to indicate hydration degree of binders (α):

$$\alpha = \frac{\Delta w_t^{\sim 350}}{\Delta w_{390d}^{\sim 350}} \tag{9}$$

where $\Delta w_t^{\sim 350}$ is the weight loss between V60 to 350 °C from paste at the corresponding time (t) and $\Delta w_{390d}^{\sim 350}$ is the weight loss in the same range from pastes cured in moisture condition for 390 days.

Fig. 5b shows Nw in the well-hydrated paste (particles with D < 1 mm curing under moisture condition for 390 days at 20 °C). The bound water in OPC, FA blended, SL blended, and ternary pastes is 0.245, 0.188, 0.204 and 0.164 g/g binder, respectively. P045, P145 and P245 have the similar content of Nw at V60-350 °C, and P345 has the lowest Nw at this range after 390 days. The differences in reactivity of OPC, FA and SL can be effectively distinguished by the hydration degree evolution (see Fig. 6a). SL and FA show different reactivities evidently after 3 days and the gap increases with hydration time, while the difference between OPC and SL decreases from 3 to 12 days. An increase of *w/b* from 0.35 to 0.45 enforces a significant enhancement in hydration of OPC after 1 day. *w/b* has weak effect on the hydration degree of the blended pastes before 12 days. The water loss between 350 and 500 °C was normalized to OPC content and presented in Fig. 6b. This part of water is typically ascribed to the decomposition of portlandite. An increase in *w/b* facilitates the precipitation of portlandite especially after 3 days. Although FA has a much lower reactivity than SL, it has a greater inhibition on the precipitation of portlandite than SL. Blending of LL increases the portlandite content compared with SL binary pastes. Adu-Amankwah et al. [62] reported the same effect from LL on content of portlandite, and they claimed that it was because a less calcium is needed to form the calcium-rich AFm phases as more Al is bound in the C–S–H of LL ternary paste.

3.3. Electrical conductivity of pore solution

Pore solution is the main conductive component in the paste and the ionic conductivity of solution depends on species of ions and the concentration of them. The concentration of the highly soluble alkalis can be calculated with the evaporable water content from the last section. The volume of Epw (V*epw*) can be calculated as:

$$V_{epw} = \frac{m_{epw}}{\rho_{epw}} = m_b \times \varphi_{epw} \tag{10}$$

where m_{epw} (g) is the mass of Epw, ρ_{epw} is the density of water (1 g/cm^3) and m_b is the mass of binder in paste.

The concentration of K^+ and Na^+ in pore solution can be calculated by Eq. (11), based on two assumptions: firstly, the alkalis are dissolved completely within the first few minutes after water mixing; secondly, the solvent exchanged water including interlayer water is classified as conductive "pore solution". The latter assumption is reasonable because Lothenbach and Nonat [61] proposed that part of alkalis absorbed in the interlayer space.

$$C_i = \frac{m_b \times \delta_{ic}}{V_{epw}} = \frac{\delta_{ic}}{\varphi_{epw}} \tag{11}$$

where C_i denotes the concentration of alkalis, i represents K^+ or Na^+, and δ_{ic} is the mole concentration of chemical composition in binder as presented in Table 1. For the SL blended paste, we use the effective mole concentration ($\delta_{iblended}$) and it needs to be modified by Eq. (12) [63], because the alkalis in SL is not as soluble as those in OPC.

$$\delta_{iblended} = \left(1 - 1.8 \times \left(\frac{m_s}{m_b}\right)^2\right) * \left(\delta_{is} \times \frac{m_s}{m_b} + \delta_{ic} \times \frac{m_c}{m_b}\right) \tag{12}$$

where m_s and m_c represents the weight of SCMs and cement in paste, respectively. δ_{is} is the mole concentration of alkalis in SCMs. K_2O and Na_2O in FA are hardly soluble during the early hydration, so the contribution of alkalis from FA is negligible (m_s =0). In addition to K^+ and Na^+, the high conductive ions in pore solution comprise OH^-, Ca^{2+}, SO_4^{2-} and Cl^-. The concentration of sulfate can be roughly approximated by Eq. (13) according to Ref. [64] where the value of α is 0.06 L/mol. Because of the low content of Cl in binder (see Table 1), its concentration in pore solution is negligible. The Ca^{2+} concentration was assumed to be constant as 25 mmol/L which is close to the typical saturated value during early hydration [28]. OH^- concentration was then calculated from charge balance by Eq. (14):

$$c_{SO_4^{2-}} \approx \alpha (c_{K^+} + c_{Na^+})^2 \tag{13}$$

$$c_{OH^-} = c_{K^+} + c_{Na^+} + 2c_{Ca^{2+}} - 2c_{SO_4^{2-}} \tag{14}$$

The electrolyte conductivity of pore solution (σ_{ps}) can be expressed as a sum of molar conductivity of each ion species (i) [65]:

$$\sigma_{ps} = \sum_i z_i \lambda_i c_i \tag{15}$$

where z_i and c_i are the valence and molarity of "i" species, respectively. λ_i is the equivalent conductivity that is related to the ionic strength (I_M) and conductivity coefficients (G_i) for the high concentration of ions in pore solution as [33]:

$$\lambda_i = \frac{\lambda_i^0}{1 + G_i \times I_M^{1/2}} \tag{16}$$

λ_i^0 is the equivalent conductivity of ionic species at infinite dilution. This value for the relevant ions at 20 °C was obtained from the literature [66] by interpolation. G_i of specific ions refers to the value in Ref. [33]. The I_M has the following definition:

$$I_M = \frac{1}{2} \sum_i z_i^2 c_i \tag{17}$$

Electrical conductivity of pore solution was calculated by Eq.(10)–(17) based on the chemical composition in Table 1 and Epw content at corresponding hydration time (in Fig. 5). By substituting the concentration of ions in the squeezed pore solution from Refs. [29,67] into Eq. (15)–(17), we calculated conductivity of pore solution of corresponding mix from literatures. The evolution of conductivity was fitted by Hill function, and the optimized parameters and function expressions are presented in Table 3.

Fig. 7a shows the calculated conductivity and fitted line of 11 samples. Electrical conductivity of pore solution decreases as the increase in *w/b* because a higher *w/b* introduces more evaporable water into paste to lower concentration of alkali ions. Blending of SCMs lowers the conductivity of pore solution, and this is consistent with the data calculated based on the squeezed pore solution in published papers (see Fig. 7b). Shi [68] also found that the blending of SCMs would reduce the conductivity of pore solution. Although the FA used in Ref. [67] has a high alkali content (3.9% K_2O and 0.9% Na_2O), the concentrations of K^+, Na^+ and OH^- in the FA blended pastes are similar with that in pastes with an identical replacement of quartz. This confirms our assumption that alkalis in FA are hardly dissolvable. The measured conductivity before 2 h (see Fig. 4) is lower than the calculated conductivity of pore solution at early ages because the presence of cement particles breaks the connectivity of pore solution. The chemical composition of OPC in this study is highly similar to that of OPC used in Ref. [67], so the calculated conductivity evolution of P055, based on chemical composition and Epw, is close to that of OPC with *w/b* = 0.5 from the squeezed pore solution (see light blue hexagon in Fig. 7a and dashed line sphere in Fig. 7b from 4 to 288 h. The main contribution to the conductivity of pore solution comes from the OH^- which accounts for around 70% (see Fig. 7b). Electrical conductivity of pore solution keeps almost constant until it has a sharp increase after about 6 h. The fitted lines in Fig. 7a

Table 3
The fitting results of pore solution conductivity depending on time by Hill function.

Sample	Expression (σ_{ps}(t))	End value(mS/cm)	R^2
P035	$\sigma_{ps} = 95.6+(165.9–95.6) \times \tau^{1.86}/(\tau^{1.86}+144.4)$	165.9	0.998
P045	$\sigma_{ps} = 76.9+(131.3–76.9) \times \tau^{2.25}/(\tau^{2.25}+512.0)$	131.3	0.998
P055	$\sigma_{ps} = 65.2+(102.9–65.2) \times \tau^{2.25}/(\tau^{2.38}+503.0)$	102.9	0.987
P135	$\sigma_{ps} = 63.1+(104.4–63.1) \times \tau^{1.5}/(\tau^{1.5}+108.8)$	104.4	0.996
P145	$\sigma_{ps} = 51.6+(96.0–51.6) \times \tau^{0.75}/(\tau^{0.75}+27.0)$	96.0	0.995
P235	$\sigma_{ps} = 75.2+(149.6–75.2) \times \tau^{0.96}/(\tau^{0.96}+31.4)$	149.6	0.990
P245	$\sigma_{ps} = 61.7+(114.5–61.7) \times \tau^{1.13}/(\tau^{1.13}+116.9)$	114.5	0.992
P255	$\sigma_{ps} = 52.4+(111.6–52.4) \times \tau^{0.75}/(\tau^{0.75}+60.3)$	111.6	0.96
P335	$\sigma_{ps} = 61.4+(133.3–61.4) \times \tau^{0.60}/(\tau^{0.60}+16.7)$	133.3	0.998
P345	$\sigma_{ps} = 50.6+(86.9–50.6) \times \tau^{0.88}/(\tau^{0.88}+35.8)$	86.9	0.995
P355	$\sigma_{ps} = 43.8+(78.0–43.8) \times \tau^{0.86}/(\tau^{0.86}+84.9)$	78.0	0.994

show the same trend as the evolution of value calculated from the squeezed pore solution in Fig. 7b. These suggest that Eq. (10)–(17) can effectively quantify the specific conductivity of pore solution with no need for extracting the solution from paste and the further test evolving with any expensive equipment (ICP-OES, IC, AAS [28]).

3.4. Real-time evolution of microstructure

3.4.1. Real-time formation factor

The formation factor (F) was initially defined by Archie [69] as a fundamental property to relate the resistivity of sandstone with its permeability or porosity. Because the hardened cement-based materials has the similar porous nature as sandstone, F is widely used in pastes or concrete by the definition with Eq. (18) [70,71]:

$$F = \frac{R_p(t)}{R_{ps}(t)} = \frac{\sigma_{ps}(t)}{\sigma_p(t)} \tag{18}$$

where $R_p(t)$ and $\sigma_p(t)$ is the resistivity and conductivity of the saturated cement-based materials, respectively. $R_{ps}(t)$ and $\sigma_{ps}(t)$ is the resistivity and conductivity of bulk pore solution respectively. t is the curing age.

Fig. 8 presents the evolution of F in pastes up to 180 days. F initially keeps near constant for a certain time (~2–9 h), and the duration of this period varies due to the blending of SCMs and different w/b (see Fig. 8a). The initial F are larger than 1 and it generally deceases with the increase of w/b. It is followed with a sharply increasing stage after the constant period. The similar declining point was found in the ultrasound test due to the percolation of solid at the setting time [1,72]. The effect of w/b on the F is magnified by the hydration in the fast growth period. The ratio of F in pastes with $w/b = 0.35$ to pastes with $w/b = 0.45$ is 1.90, 2.57, 3.90 and 2.05 for OPC, FA, SL and ternary system, respectively. F of P035 and P045 keep increasing with a slow rate from 12 to 180 days, but that of P055 shows an interesting decrease from 28 to 180 days. The FA blended pastes have the highest increase in F compared with other pastes from 12 to 180 days so that they have the highest value at 180 days among pastes with the same w/b. F of the SL blended pastes shows an evident increase after 12 days, but its growth rate is much lower than the FA pastes. The differences in F of SL binary pastes and ternary pastes with the same w/b is negligible after 28 days.

Fig. 8b illustrates the comparison of F of pastes with $w/b = 0.35$. OPC paste has the highest F at early age, but F of SL blended paste exceeds that of OPC after 36 h. LL reduces the growth rate of F in the first 36 h, but F of ternary pastes climbs up to exceed that of OPC at 110 h. The P135 has the lowest F because of the low reactivity of FA at early age. With an increase of w/b to 0.45, the difference between OPC and SL blended paste is magnified in the first 24 h. F of P245 and P345 exceeds that of P045 at 110 and 140 h respectively, which is much longer than this time for paste with w/b of 0.35 (36 and 110 h, respectively). An increment of w/b to 0.55, furthermore, intensifies the inhibition effect of SL and LL on the growth rate of F in the first 24 h. P255 and P355 exceed the P055 at the same time of 175 h.

F also relates to the ion diffusivity and pore connectivity as this equation [70,73]:

$$F = \frac{1}{\Phi\beta} \tag{19}$$

Φ is the porosity and β is the index of pore connectivity. Herein, the water porosity was used to calculate the pore solution connectivity, and it is defined as:

$$\Phi_e = \frac{V_{epw}}{V_p} = \frac{m_1 - m_e}{m_1 - m_0 - m_v} \tag{20}$$

V_p is the volume of the hardened paste. With the data of water distribution (Fig. 5) and F, the pore solution connectivity (β) was calculated (see Fig. 8c–d). An increment in w/b increases this value in pastes. As hydration proceeds, the β deceases dramatically from water addition to 24 h. Although the volume of Epw in SL blended systems (see Fig. 5 P235/245, P335/P345) is higher than that in OPC pastes with identical w/b, β of the SL blended pastes is lower than OPC. This results in a higher

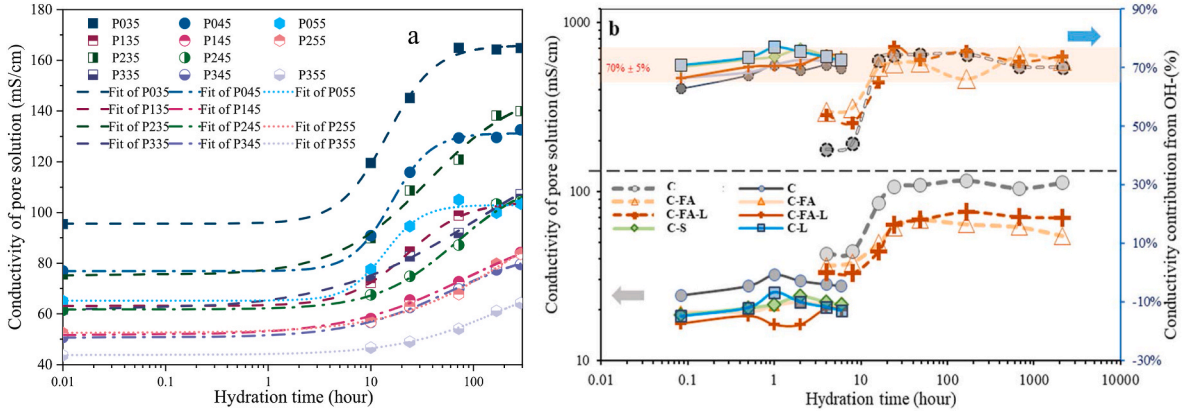

Fig. 7. Calculated conductivity of pore solution. (a)- the values in this paper. (b)- the conductivity value calculated based on the tested concentration of squeezed pore solution from literatures (solid line from Ref. [29] with w/b = 0.75, dash line from Ref. [67] with w/b = 0.5, C: OPC; FA: FA; S: SL; L: LL).

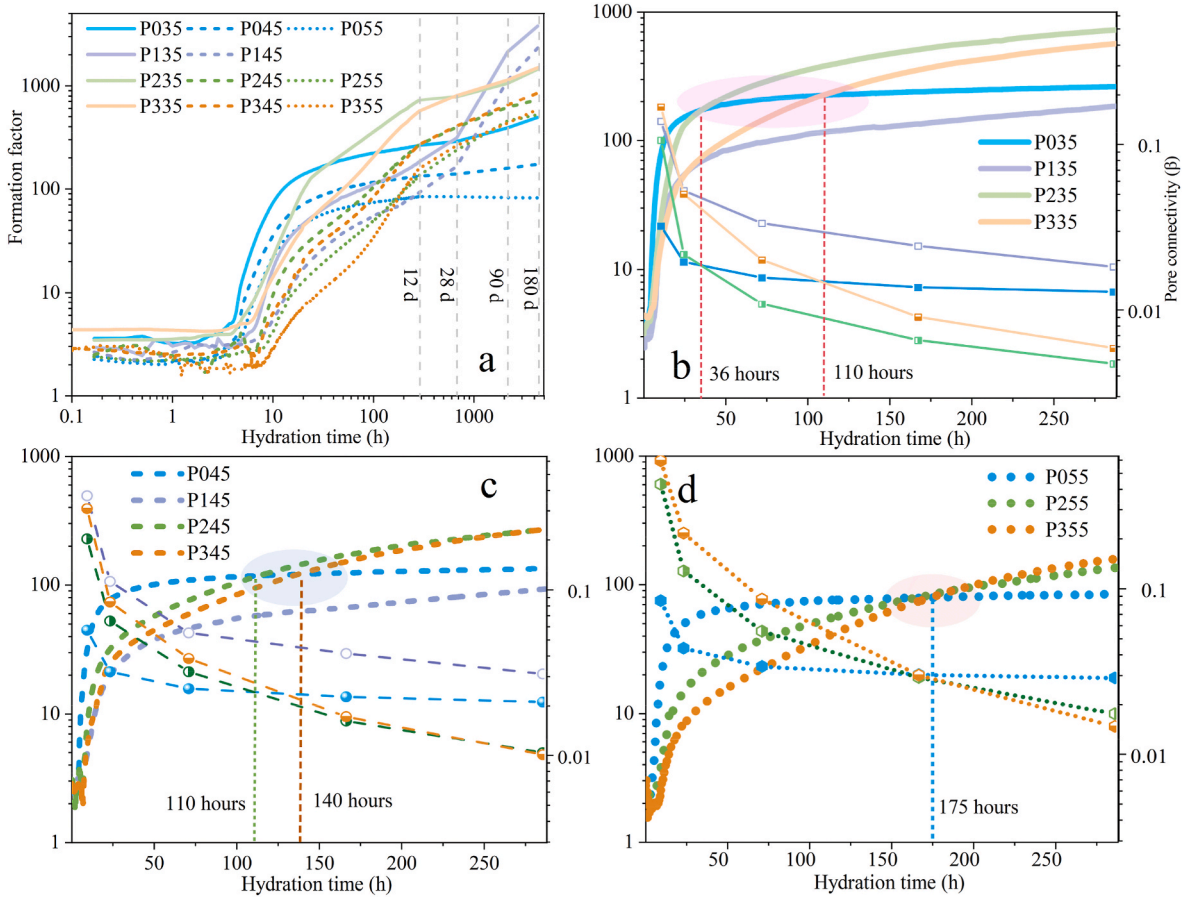

Fig. 8. Evolution of formation factor and pore solution connectivity with hydration time.

F of SL blended paste. It implies that the differences in *F* between various binder systems mainly derive from discrepancies in β.

3.4.2. *Average growth rate of F*

For a further detail analysis of the growth rate of formation factor, the average growth rate of *F* (*a-F*) is defined as:

$$a-F=\frac{F(t)}{t} \tag{21}$$

where $F(t)$ is the *F* at hydration time *t*. The *a-F* of pastes is presented in Fig. 9. The shape of *a-F* curve is similar with the typical shape of heat release rate curve. By referring to the category based on the heat release [43], the evolution of *a-F* of OPC paste can be classified into three periods as well. It includes "to the end of low-rate period" (period I), "accelerate period" (period II) and "deceleration period" (period III). For the blended paste, one more peak occurs after the main peak and it belongs to the fourth period (period IV).

Period I: *a-F* has a sharp decrease in the beginning. It reaches the lowest value that keeps almost constant for a period. The hydration of OPC in this period involves the dissolution of minerals, the precipitation of ettringite and nucleation of C–S–H [74]. However, these reactions have few effects on the volume and connectivity pore solution, so *F* is almost constant at this period (see Fig. 8a). Dividing *F* with time gets a sharp decline in *a-F*. The continuous precipitation of ettringite and C–S–H gradually strengthens the connectivity between particles. This reduces the connectivity of pore solution, so the *F* may have a slow linear-like growth leading to a constant *a-F*. An increase in *w/b* increases the duration of period I and decreases *a-F* at the end of this period. Blending of SCMs reduces *a-F* and prolongs this period. We define the inflection point of *a-F* as the end of period I (see dash line in Fig. 9c and d), the duration of period I was presented in Table 4.

Period II: *a-F* has a sharp increase in this period. The hydration goes into period with a rapid growth of hydration products (ettringite, C–S–H and portlandite [74,75]) after the low *a-F* period. It increases the connectivity between the solid particles to block the connection of pore solution. Meanwhile, the water transfer from free water to chemically bound to reduce the content of Epw, thus also decreasing the connectivity of pore solution. *a-F* is an effective index for demonstrating the hydration reactivity of binders with the same *w/b*. Fig. 9 a and b show that OPC has the highest *a-F* in period II due to its higher reactivity compared with SCMs (FA, SL and LL). Although the hydration degree of FA and SL blended paste has few differences in the first 24 h (Fig. 6a), *a-F* of SL blended is much higher than FA. It implies that the interaction and links between the unhydrated particles is not only controlled by the precipitation of products on surface but also double layers structure between solid and pore solution. The dissolution of FA is typically lower than SL [76], so there is fewer specifically absorbed anions (K^+, Na^+ or Ca^{2+}) and secondary water [77] on FA surface than SL. Moreover, the absolute zeta potential of FA is much higher than SL and cement in $Ca(OH)_2$ solution [77], so it means that the stable distance between the FA and other particles are larger than that of SL and other particles. This weakens the connection between solids to bring a higher connectivity of pore solution.

Period III: *a-F* shows a decreasing trend after the period II, and this is due to a reduction in the growth rate of hydration products as well as the water consuming rate. The main peak of *a-F* of OPC pastes is at 12.6, 14 and 14 h for w/b of 0.35, 0.45 and 0.55, respectively (see Fig. 9a and b), which is close to the main peak of heat release rate (12–14 h for OPC [43]) form OPC pastes. The blending of SCMs delays the main peak to 16–20 h and this interval is also close to the time for the main peak of

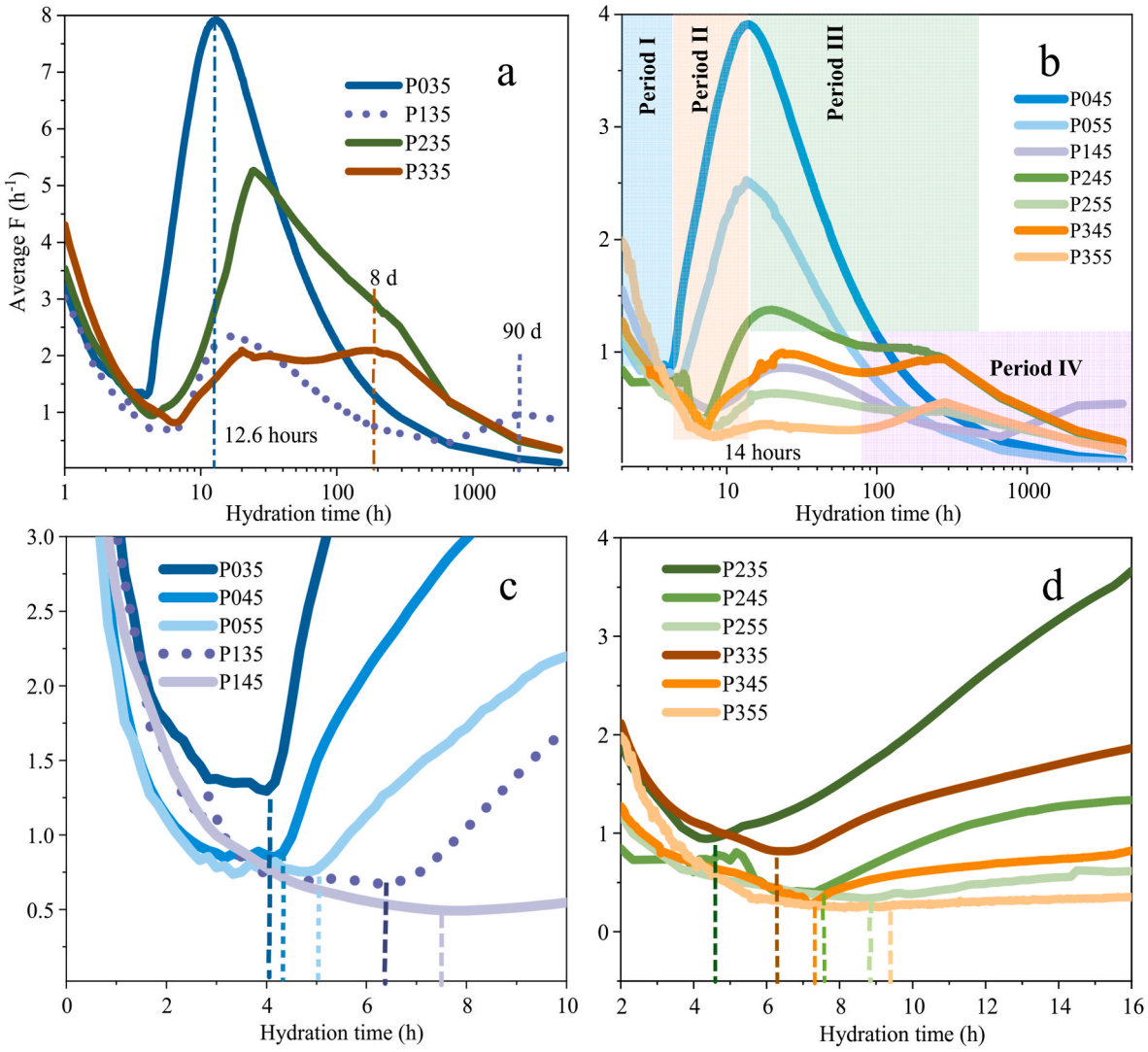

Fig. 9. Evolution of *a-F* of pastes with hydration time.

Table 4
Setting time and inflection points of *a-F* from fresh pastes.

Sample	Time/h		
	Initial setting	Final setting	Inflection point of a-F
P035	2.82	4.37	4.07
P045	3.62	5.02	4.38
P055	4.14	6.80	5.04
P135	4.06	6.65	6.35
P145	4.85	7.17	7.30
P235	2.99	5.72	4.60
P245	4.20	7.92	7.50
P255	4.49	9.50	8.80
P335	3.08	6.12	6.25
P345	4.13	7.97	7.33
P355	5.82	10.23	9.30

heat release in OPC with SL and FA [78]. An increase in *w/b* has minor influences on the main peak position especially from 0.45 to 0.55. SCMs decrease the declining rate of *a-F* and they even induce one more peak. Interestingly, the inhibiting effect on the precipitation of portlandite from FA is higher than that from SL (Fig. 6b), but the *a-F* of FA paste is much lower than that for SL pastes. This may be owing to the phenomenon that FA absorbs Ca^{2+} on its surface during the dissolution process [50,79,80], and these Ca ions would not necessarily precipitates as portlandite or C–S–H.

Period IV: This period corresponds to one new peak during the deceleration of *a-F*. Because the latent hydraulic reactivity has been activated after 3 days, the reaction of SL induces a further breaking of the pore connectivity, namely refining the pore size. This latent hydraulic reactivity can be observed from the increment in the differences between the normalized portlandite content in OPC and SL blended paste (see Fig. 6b). The time for the second peak of *a-F* in P235, P245 and P255 is about 8–12 days, and this period corresponds to a quick increase in the reaction degree of SL according to Ref. [80]. The reaction of FA is normally activated much later than 10 days [7,80], so the second peak of FA blended pastes occur at about 90 days in this study. An increase in *w/b* seems to delay the occurrence of this peak.

3.4.3. Setting time

Fig. 10 shows the penetration depth in fresh pastes tested by the Vicat needle. The initial and final setting time were determined referring to ASTM C191-08 standard and the results are presented in Table 4. An increase in *w/b* prolongs both the initial and final setting time. This delaying effect is more evident on final setting than initial setting. Penetration depth of ternary pastes fluctuate under all *w/b* conditions (Fig. 10a). The blending of SCMs inhibits the deceasing rate of the penetration depth (see Fig. 10b–d), and FA has the strongest inhibiting effect. Lootens et al. [81] found the analytical correlation between the

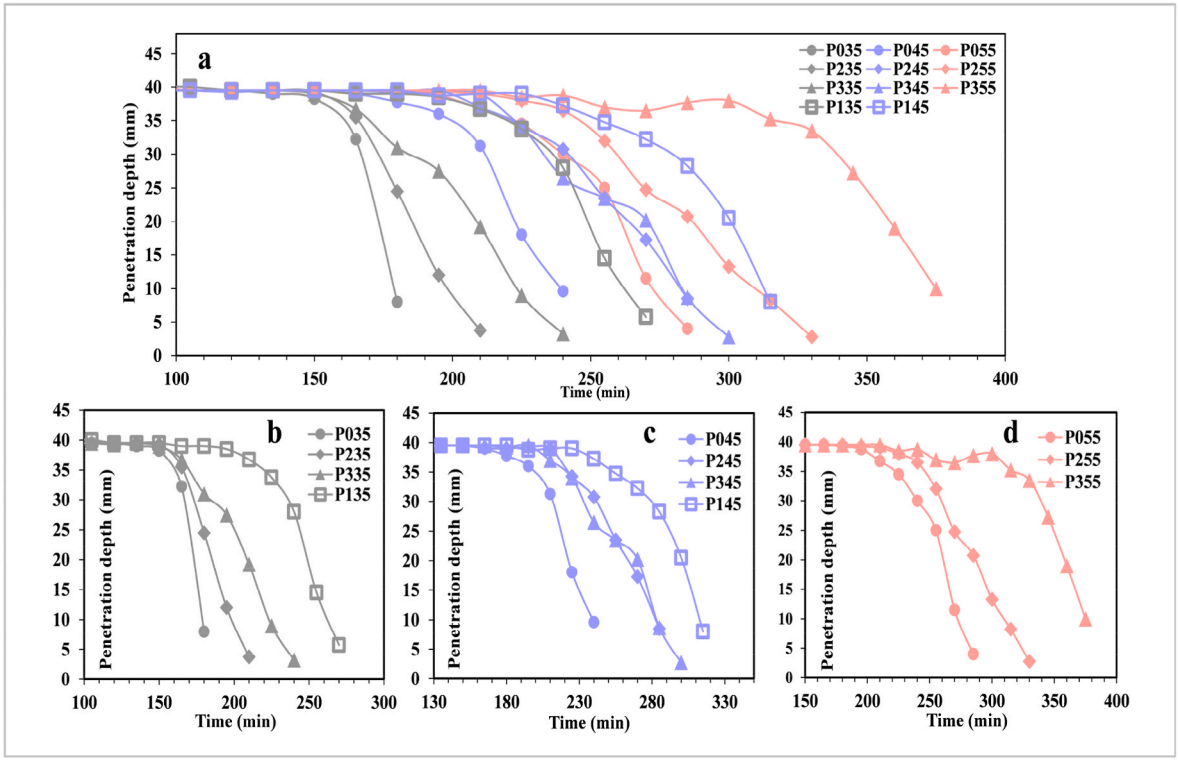

Fig. 10. Penetration depth of Vicat needle in pastes at different hydration times.

penetration depth and yield stress of materials. A penetration depth of 25 mm from a needle used in ASTM C191-08 can be associated to a yield stress of order 40 kPa. The spherical shape of FA mitigates the inter-particle surface friction [82]. Moreover, the higher absolute zeta potential of FA leads to a larger distance between particles compared to SL. Therefore, FA paste needs a longer time to gain the enough density of hydration products to reach the yield stress for setting than SL blended paste. The dilution effect from SL also induces pastes to take a longer time to gain the critical yield stress for the initial setting than the plain pastes. Table 4 illustrates that both initial and final setting have a positive correlation with inflection point of *a-F*. It will be further detailed in the discussion part.

3.4.4. Time-dependency of chloride migration coefficient and F

The proper evaluation of chloride migration coefficient is important for service life modelling. Chloride migration coefficient is a time-dependent parameter that decreases with the curing time following an empirical power function [83–86], owing to the continuous hydration of binder. Table 5 shows the chloride migration coefficient of pastes tested by rapid chloride migration (D_{RCM}) at different curing time. D_{RCM} of pastes show an unsurprising decrease with the curing time except for P055. D_{RCM} increases with the increase in *w/b*, but the *w/b* has a weak influence on D_{RCM} of SL binary paste at 180 days. The blending of SCMs decreases the chloride migration in pastes, and this effect is more evident in pastes with longer hydration time and higher *w/b*. D_{RCM} of P055 shows an interesting increase with hydration time after 28 days. The similar deviation was detected in some previous investigations [84, 85] as well. OPC based concrete might have a higher chloride migration coefficient at later age when the *w/b* is rather high (>0.5).

Eq. (19) indicates that the inverse of *F* (*1/F*) correlates to the pore connectivity and porosity, so the evolution of *1/F* was used to compare with D_{RCM}. Fig. 11a shows that a minor increase in the 1/*F* can also be observed in P055 after from 28 to 90 days. This implies the increase in D_{RCM} is due to the changes of structure in hardened pastes. The dependency of D_{RCM} on time is similar with the dependency of *1/F* on time in OPC and FA blended pastes (see Fig. 11 a and b). The effect from *w/b* on the D_{RCM} is close to its effect on *1/F* in these two binder systems. Both the D_{RCM} and *1/F* in the slag blended pastes show a declining trend with the increase in curing time, but the decreasing rate of D_{RCM} is much higher than that of *1/F* especially for pastes with *w/b* of 0.35 and 0.45. Because the *1/F* is measured from pastes under the sealed curing, the hydration rate of pastes with *w/b* of 0.35 and 0.45 is limited due to the lack of liquid water at later age, thus leading to the slow decrease of *1/F* after 90 days. However, D_{RCM} was tested from samples under the water curing so the later-age hydration is higher than the sealed samples. This causes a higher decrease in D_{RCM} of the water curing samples than that in *1/F* of the sealed curing samples (see Fig. 11 c and d).

Table 5
The D_{RCM} of pastes cured to 28, 90 and 180 days.

Time/days	Chloride migration coefficient ($\times 10^{-12}$ m^2/s)										
	P035	P045	P055	P135	P145	P235	P245	P255	P335	P345	P355
28	8.02	15.56	21.08	8.90	11.35	5.12	5.82	7.29	5.79	5.39	6.40
90	5.84	11.67	26.28	2.27	3.67	3.17	3.85	4.52	2.70	3.64	3.81
180	3.52	10.46	26.15	0.84	1.51	2.50	2.60	2.91	1.76	1.94	3.71

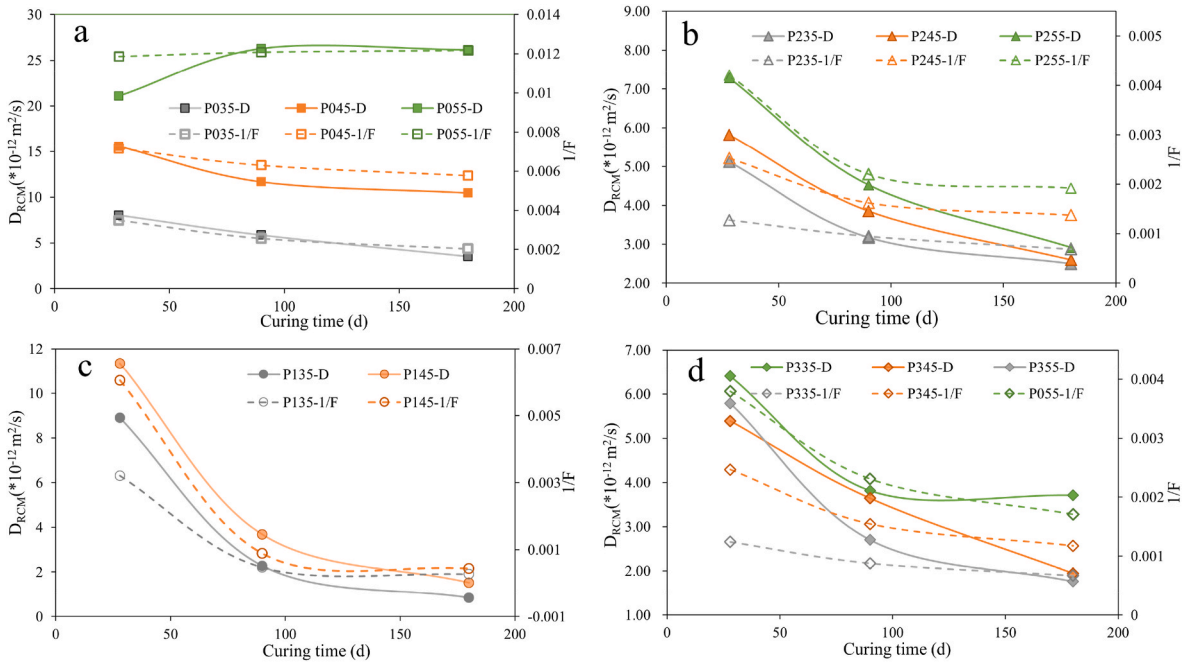

Fig. 11. The evolution of chloride migration coefficient (solid scatters) and inverse of *F* (the hollow scatters) with hydration time: a- OPC pastes; b- The FA blended pastes; c- The slag blended pastes; d- The ternary pastes.

4. Discussion

4.1. Correlation between setting time and formation factor

The setting of cement-based materials has been indicated by many test methods [87], and the change of electrical properties is one of the major index [88]. It can be observed that the decreasing rate of penetration correlates to the growth rate of *F* with the comparison between Figs. 9 and 10. The inflection time of *a-F* is positively related to the setting time as shown in Table 4. Setting of cement paste is generally understood as a percolation process in which intersection of hydration products on particles surface leads to the formation of clusters, and which eventually join into a continuous elastic network [1]. In OPC with normal aluminates content, the setting of cement is mainly controlled by a formation of sufficient C–S–H on particles surface [89,90]. The increasing precipitation of C–S–H from period I to II (in Fig. 9) results in the percolation of the links built by the overlapping of C–S–H on the surfaces of particles.

Many previous researches [91–93] noticed a reduction of conductivity of paste during setting, however, lack of building any mathematic relation between electrical properties and setting time. The *a-F* in this paper represents the structure building rate, so the change of it is effective to indicate the setting of pastes. Fig. 12 shows that the inflection point of *a-F* has a good linear correlation with the final setting time regardless of types of binder or *w/b*. The linear correlation is not so general between the inflection point and initial setting time for all pastes, but the correlation is good in pastes within the same binder system (Fig. 12 arrow line). This may be due to the differences in particles size distribution (or surface nature of the particles in solution) between cement and SCMs. Moreover, it should also be noted that in the standard test (ASTM C191-08, Vicat) the points for initial setting are arbitrary chosen. Generally, the change of *a-F* during hydration is a good index for setting of pastes.

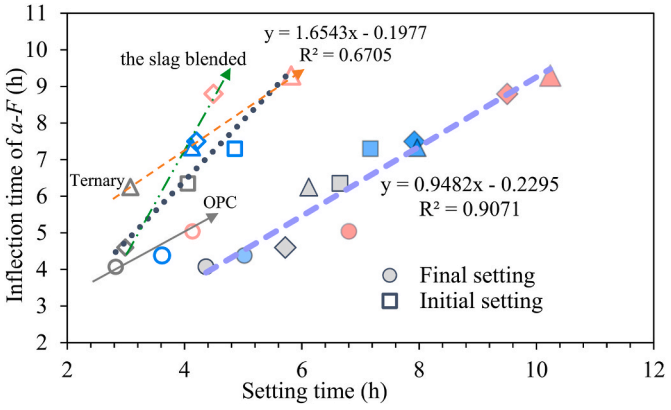

Fig. 12. Correlations between setting time and inflection point of a-F. OPC, FA blended, SL blended and ternary paste are presented with circle, square, rhombus and triangle respectively. The grey, blue and rose color correspond to *w/b* of 0.35, 0.45 and 0.55 respectively. (For interpretation of the references to color in this figure legend, the reader is referred to the Web version of this article.)

4.2. Percolation theory understanding the relation between Epw and formation factor

Water plays a critical role during the hydration process. It works not only as a "porter" to carry the ions out of raw minerals into solution but also as a key component to build the chemical structure of hydration products. Pore solution is also the main basis of current transmitting through the cement-based materials. The electrical conductivity of paste is affected by many intrinsic factors during hydration as shown in Fig. 1. To simplify the system at the specific hydration degree, the composition in pastes can be classified into two main phases: the insulative (dry solid) and conductive component (liquid solutions). Archie [69] found a power function relation between the volume percentage of conductive saline (Φ) and the formation factor *F* of gas sand, and it was further stated as the general form [94]:

$$\frac{\sigma_p}{\sigma_{ps}} = 1 \Big/ F = a^{*}\varphi^{n} \tag{22}$$

where *a* is non-uniform constant, *n* is the shape factor. After an extension

of the percolation theory of networks to the continuum cases [95,96], the conductivity shows a general relation as a formula similar to Archies' law:

$$\sigma_p = a * \sigma_{ps} * (\varphi - \varphi_c)^m \quad (23)$$

After the substitution of conductivity with *F*, we get:

$$F = 1 / a * (\varphi - \varphi_c)^{-m} \quad (24)$$

herein, we assume that the conductive component includes the ions in the pore water and the layer water, hence φ is the volume of Epw (φ_e). φ_c is the critical value for the percolation of conductive component. *m* is the shape factor as in Archies' law and *a* is a constant. Fig. 13 demonstrates the raw data and the regressed curve, and Table 6 shows the optimum parameters. *F* correlates perfectly with Epw through the general percolation theory with respect to different binder type (see Fig. 13a and R^2 in Table 6).

Binder types have impact on the shape factor and threshold for percolation, so a general fitting with all binder types is not so good with $R^2 = 0.74$. The single-shaped particle system has a lower shape factor than the system with a complex shape mixing, such as the sand and chalk with a value of 1.6 but the calcium montmorillonite with 3.28 [94]. FA has a uniform spherical shape, so it will reduce the shape complexity of binder particles resulting in the lowest shape factor ($m = 1.52$). LL has the granular shape like sand so that it reduces the shape factor. Comparing to OPC, the higher *m* value in the SL blended paste indicates that SL binder system has a more complex shape combination than the others.

The values of percolation threshold for solution in OPC, FA, SL and ternary blended pastes are 0.157, 0.242, 0.223 and 0.256, respectively. This means that plain OPC paste needs the lowest volume of solution to have a percolation, which in turn implies that it has the highest pore connectivity compared to the blended system. Gui et al. [39] found that FA and SL refined the pore structure to decrease the pore connectivity in pastes, thus reducing the gas permeability. The refinement effect from SL and FA also increase the chloride resistivity (see Table 5 and in Refs. [96,97]). According to lattice model for percolation [98], the site threshold values for face centered cubic and body centered cubic is 0.198 and 0.245 respectively. Therefore, it implies that the blending of SL and FA may refine the pores spatial packing state, which is worthy of consideration for the future modelling.

4.3. The relationship between D_{RCM} and electrical properties

The relationship between electrical properties and chloride migration coefficient were discussed in some previous publications [40,99,100]. Tong and Gjørv [99] empirically found a quadratic relation between the electrical conductivity and chloride migration coefficient. However, some investigations [40,100] also reported a linear correlation between these two parameters. Theoretically, the diffusivity of ions in the porous materials correlates to *F* and electrical conductivity as Eq. (25) [70,73]. D_p and D_{ps} are the diffusivity of the ions in paste and bulk pore solution, respectively.

$$D_p = \frac{D_{ps}\sigma_p}{\sigma_{ps}} = \frac{D_{ps}}{F} \quad (25)$$

Fig. 14 presents the correlations between the electrical properties and D_{RCM} in this study. It shows a linear relationship between the electrical conductivity and D_{RCM} in pastes. A better linear correlation is detected between D_{RCM} and $1/F$ with a $R^2 = 0.98$ in Fig. 14b compared with $R^2 = 0.96$ in Fig. 14a. The difference value between the regressed and the measured D_{RCM} is presented in Fig. 14c. It shows that the residual in regression based on $1/F$ is apparently smaller than that in the regression based on electrical conductivity. The correlation between the D_{RCM} and σ_p is not quite linear because of the effect from conductivity of pore solution as presented in Eq. (25). Moreover, the conductivity of pore solution is largely influenced by the saturation degree according [101] and as shown in Fig. 7. The chloride migration is mainly controlled by pore structure instead of concentration of pore solution. The slope of the regression line between the D_{RCM} and $1/F$ is 2.037×10^{-9} m^2/s, and this value is very close to the coefficient of chloride migration in the dilute solution (2.03×10^{-9} m^2/s [102]). Therefore, the real-time monitored electrical properties are effective to indicate the chloride migration coefficient in hardened cement pastes especially based on the $1/F$. This parameter can be used to calculate the chloride migration coefficient in pastes, including the effect from the SCMs and hydration time (see Figs. 11 and 14).

Table 6
The regressed parameters based on Eq. 24

Sample	Expression	*a*	Φ_c	*m*	R^2
P0	$F = 1/0.246 \times (\Phi_e\text{-}0.157)^{-2.11}$	0.246	0.157	2.11	0.98
P1	$F = 1/0.498 \times (\Phi_e\text{-}0.242)^{-1.52}$	0.498	0.242	1.52	0.93
P2	$F = 1/0.806 \times (\Phi_e\text{-}0.223)^{-2.35}$	0.806	0.223	2.35	0.99
P3	$F = 1/0.578 \times (\Phi_e\text{-}0.256)^{-1.82}$	0.578	0.256	1.82	0.97
PA	$F = 1/0.129 \times (\Phi_e\text{-}0.279)^{-0.98}$	0.129	0.279	0.98	0.74

5. Conclusions

A simple conductivity test setup was designed for a real-time monitoring of the hydration and microstructure evolution of pastes with various *w/b* and binder systems. It can be used as an in-situ test and even

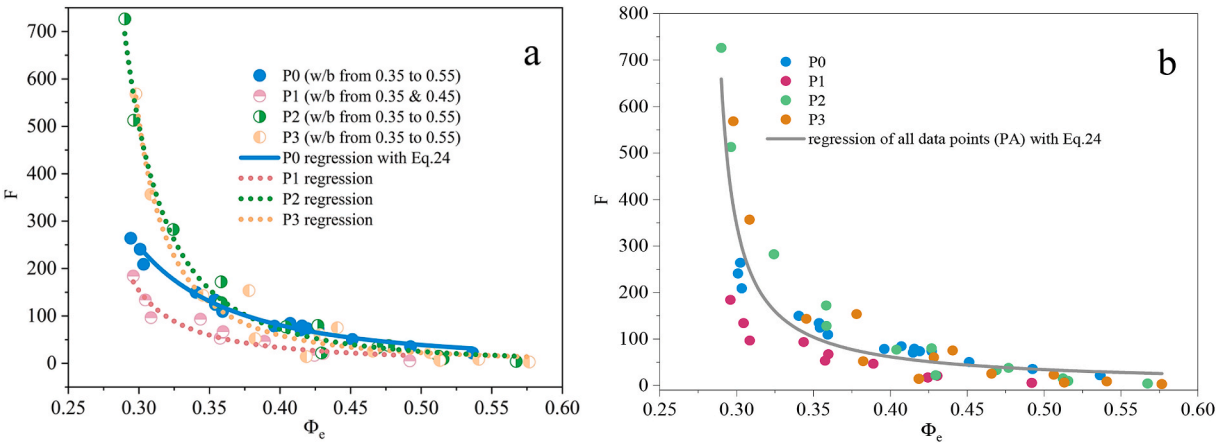

Fig. 13. Relationship between the Epw and *F*. P_0, P_1, P_2 and P_3 correspond to OPC, FA, SL and ternary blended pastes, respectively. a-data with respect to binder type; b-the regression result regardless of binder type.

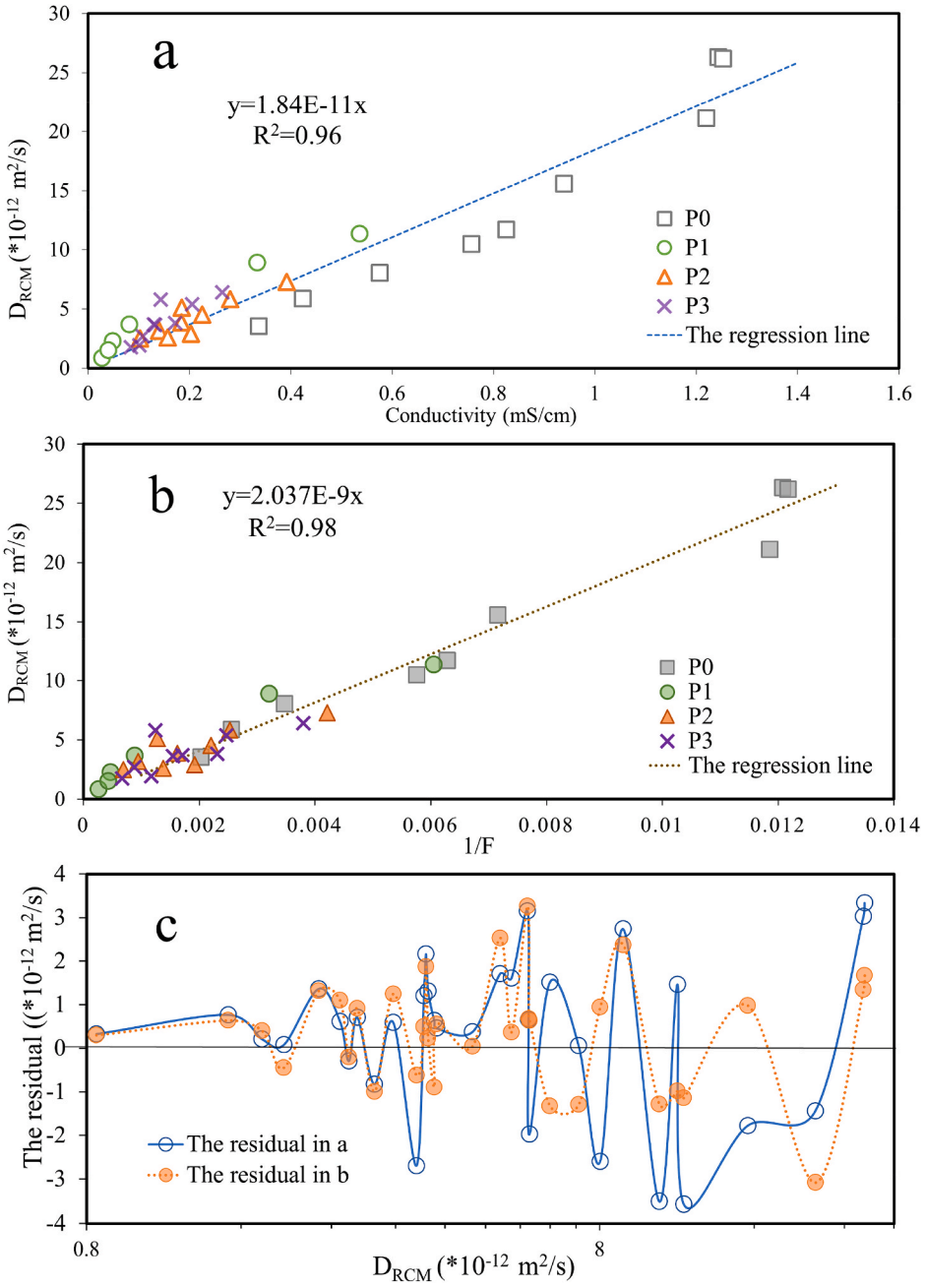

Fig. 14. The regression of chloride migration coefficient and electrical properties in pastes: a- Conductivity and D_{RCM}; b- D_{RCM} and $1/F$; c-the differences between the regression line and measured data.

for the on-site monitoring in large scale. The distribution of Epw and Nw can be easily determined with the procedure proposed in this paper. Water content from the developed procedure gives data for calculating the conductivity of pore solution based on the chemical composition of binders, without any needs for squeezing the pore solution out of the paste. With the measured conductivity of paste and calculated conductivity of pore solution, the real-time *F* and *α-F* was defined for a deep analysis of hydration process and pore structure.

The evolution of conductivity closely relates to the chemical reaction process. The differences in *F* of pastes with various binders are mainly derived from the pore connectivity. *α-F* is an effective index for indicating the structure development rate in pastes. The shape of *α-F* curve is similar with that of heat release, so it contains a first peak, a main peak and the later stable period in OPC pastes. Another peak shows in the hydration of paste blended with SL and FA due to the latent hydraulic reaction of SL and pozzolanic reaction of FA. The evolution of *α-F* in the blended pastes was correspondingly classified into four periods. The rapid growth of C–S–H induces an inflection point of *α-F* from period I into II, which can perfectly indicate the final setting time.

The *w/b* impacts the electrical conductivity, *F*, and *α-F* of pastes. An increase in *w/b* lowers the alkali concentration in pore solution, leading to a lower electrical conductivity. However, it increases the connectivity of pore solution to reduce *F*. An increment in *w/b* also reduces *α-F* of pastes, and the *α-F* can effectively indicate the reactivity of different binders under the same *w/b* condition. Dilution effects from SCMs reduce the initial conductivity of paste mainly due to the lower alkali concentration in pore solution. SL has a weaker reduction in the conductivity of pore solution than FA and LL. Blending of SL refines the pore structure at early age, so the SL blended paste has a higher *α-F* than OPC after about 4 days. FA reduces *F* and *α-F* in the first 12 days due to its low

reactivity at early age, but the effect of its pozzolanic reaction shows after 28 days. LL increases the connectivity of pore solution. However, its filling effect on pore structure is effective after a certain hydration age.

The relation between volume of Epw and F can be well demonstrated by an extended percolation theory. This enables an in-situ evaluation of Epw through conductivity test. The real-time monitored electrical conductivity and $1/F$ can be used to estimate the chloride migration coefficient in hardened cement pastes. This study provides both useful methods and theoretical basis for the prediction and simulation of moisture content and ions (e.g. chloride) ingress in cement-based materials with a continuous long-term hydration during its service life.

Declaration of competing interest

The authors declare that they have no known competing financial interests or personal relationships that could have appeared to influence the work reported in this paper.

Acknowledgements

The authors appreciate the financial support from Swedish Research Council for Environment, Agricultural Sciences and Spatial Planning FORMAS (2018–01430) and National Key Research and Development Program of China (No. 2018YFD1101002). We also appreciate the partially financial supports from Thomas Concrete Group, SBUF (the construction industry's organization for research and development) and Cementa AB.

References

[1] G.W. Scherer, J. Zhang, J.A. Quintanilla, S. Torquato, Hydration and percolation at the setting point, Cement Concr. Res. 42 (2012) 665–672, https://doi.org/10.1016/j.cemconres.2012.02.003.
[2] P.K. Mehta, P.J. Monteiro, Concrete: Microstructure, Properties, and Materials, McGraw-Hill Education, 2014.
[3] J.J. Thomas, J.J. Biernacki, J.W. Bullard, S. Bishnoi, J.S. Dolado, G.W. Scherer, A. Luttge, Modeling and simulation of cement hydration kinetics and microstructure development, Cement Concr. Res. 41 (2011) 1257–1278, https://doi.org/10.1016/j.cemconres.2010.10.004.
[4] P.J.M. Monteiro, S.A. Miller, A. Horvath, Towards sustainable concrete, Nat. Mater. 16 (2017) 698–699, https://doi.org/10.1038/nmat4930.
[5] G. Habert, S.A. Miller, V.M. John, J.L. Provis, A. Favier, A. Horvath, K. L. Scrivener, Environmental impacts and decarbonization strategies in the cement and concrete industries, Nat. Rev. Earth Environ. 1 (2020) 559–573, https://doi.org/10.1038/s43017-020-0093-3.
[6] K. Scrivener, R. Snellings, B. Lothenbach, A Practical Guide to Microstructural Analysis of Cementitious Materials, Crc Press, 2018.
[7] K.L. Scrivener, B. Lothenbach, N. De Belie, E. Gruyaert, J. Skibsted, R. Snellings, A. Vollpracht, TC 238-SCM: hydration and microstructure of concrete with SCMs: state of the art on methods to determine degree of reaction of SCMs, Mater. Struct. 48 (2015) 835–862, https://doi.org/10.1617/s11527-015-0527-4.
[8] P.J.M. Monteiro, G. Geng, D. Marchon, J. Li, P. Alapati, K.E. Kurtis, M.J.A. Qomi, Advances in characterizing and understanding the microstructure of cementitious materials, Cement Concr. Res. 124 (2019), 105806, https://doi.org/10.1016/j.cemconres.2019.105806.
[9] H. Liu, Z. Sun, J. Yang, Y. Ji, A novel method for semi-quantitative analysis of hydration degree of cement by 1H low-field NMR, Cement Concr. Res. 141 (2021), 106329, https://doi.org/10.1016/j.cemconres.2020.106329.
[10] A.M. Gajewicz, E. Gartner, K. Kang, P.J. McDonald, V. Yermakou, A 1 H NMR relaxometry investigation of gel-pore drying shrinkage in cement pastes, Cement Concr. Res. 86 (2016) 12–19, https://doi.org/10.1016/j.cemconres.2016.04.013.
[11] R. Schulte Holthausen, M. Raupach, A phenomenological approach on the influence of paramagnetic iron in cement stone on 2D T1-T2 relaxation in single-sided 1H nuclear magnetic resonance, Cement Concr. Res. 120 (2019) 279–293, https://doi.org/10.1016/j.cemconres.2019.03.027.
[12] G. Levita, A. Marchetti, G. Gallone, A. Princigallo, G.L. Guerrini, Electrical properties of fluidified Portland cement mixes in the early stage of hydration, Cement Concr. Res. 30 (2000) 923–930, https://doi.org/10.1016/S0008-8846(00)00282-9.
[13] A. Princigallo, K. van Breugel, G. Levita, Influence of the aggregate on the electrical conductivity of Portland cement concretes, Cement Concr. Res. 33 (2003) 1755–1763, https://doi.org/10.1016/S0008-8846(03)00166-2.
[14] M. Heikal, M.S. Morsy, M.M. Radwan, Electrical conductivity and phase composition of calcium aluminate cement containing air-cooled and water-cooled slag at 20, 40 and 60 °C, Cem, Concr. Res. 35 (2005) 1438–1446, https://doi.org/10.1016/j.cemconres.2004.09.027.
[15] N. Schwarz, M. DuBois, N. Neithalath, Electrical conductivity based characterization of plain and coarse glass powder modified cement pastes, Cem. Concr. Compos. 29 (2007) 656–666, https://doi.org/10.1016/j.cemconcomp.2007.05.005.
[16] A.L.G. Gastaldini, G.C. Isaia, T.F. Hoppe, F. Missau, A.P. Saciloto, Influence of the use of rice husk ash on the electrical resistivity of concrete: a technical and economic feasibility study, Construct. Build. Mater. 23 (2009) 3411–3419, https://doi.org/10.1016/j.conbuildmat.2009.06.039.
[17] A. Poursaee, W.J. Weiss, An automated electrical monitoring system (AEMS) to assess property development in concrete, Autom. ConStruct. 19 (2010) 485–490, https://doi.org/10.1016/j.autcon.2009.12.016.
[18] E. Karmazsin, M. Murat, Study of a "solid + liquid → solid" reaction (hydration of calcium sulfate hemihydrate) by simultaneous isothermal calorimetry and electrical resistivity measurement, Cement Concr. Res. 8 (1978) 553–557, https://doi.org/10.1016/0008-8846(78)90037-6.
[19] M. Perez-Pena, D.M. Roy, F.D. Tamás, Influence of chemical composition and inorganic admixtures on the electrical conductivity of hydrating cement pastes, J. Mater. Res. 4 (1989) 215–223, https://doi.org/10.1557/JMR.1989.0215.
[20] N.B. Singh, A.K. Singh, S. Prabha Singh, Effect of citric acid on the hydration of portland cement, Cement Concr. Res. 16 (1986) 911–920, https://doi.org/10.1016/0008-8846(86)90015-3.
[21] S.A.A. El-Enein, Electrical conductivity of concrete containing silica fume, 25 (n. d.) 6.
[22] M.S. Morsy, S.A.A. El-Enein, G.B. Hanna, Microstructure and hydration characteristics of artificial pozzolana-cement pastes containing burnt kaolinite clay, Cement Concr. Res. 27 (1997) 1307–1312, https://doi.org/10.1016/S0008-8846(97)00122-1.
[23] Th.M. Salem, Sh.M. Ragai, Electrical conductivity of granulated slag–cement kiln dust–silica fume pastes at different porosities, Cement Concr. Res. 31 (2001) 781–787, https://doi.org/10.1016/S0008-8846(01)00461-6.
[24] Th.M. Salem, Electrical conductivity and rheological properties of ordinary Portland cement–silica fume and calcium hydroxide–silica fume pastes, Cement Concr. Res. 32 (2002) 1473–1481, https://doi.org/10.1016/S0008-8846(02)00809-8.
[25] T.M. Chrisp, W.J. McCarter, G. Starrs, P.A.M. Basheer, J. Blewett, Depth-related variation in conductivity to study cover-zone concrete during wetting and drying, Cem. Concr. Compos. 24 (2002) 415–426, https://doi.org/10.1016/S0958-9465(01)00073-7.
[26] W.J. McCarter, T.M. Chrisp, G. Starrs, J. Blewett, Characterization and monitoring of cement-based systems using intrinsic electrical property measurements, Cement Concr. Res. 33 (2003) 197–206, https://doi.org/10.1016/S0008-8846(02)00824-4.
[27] W.J. McCarter, T.M. Chrisp, G. Starrs, A. Adamson, P.A.M. Basheer, S. V. Nanukuttan, S. Srinivasan, C. Green, Characterization of physio-chemical processes and hydration kinetics in concretes containing supplementary cementitious materials using electrical property measurements, Cement Concr. Res. 50 (2013) 26–33, https://doi.org/10.1016/j.cemconres.2013.03.008.
[28] A. Vollpracht, B. Lothenbach, R. Snellings, J. Haufe, The pore solution of blended cements: a review, Mater. Struct. 49 (2016) 3341–3367, https://doi.org/10.1617/s11527-015-0724-1.
[29] A. Schöler, B. Lothenbach, F. Winnefeld, M.B. Haha, M. Zajac, H.-M. Ludwig, Early hydration of SCM-blended Portland cements: a pore solution and isothermal calorimetry study, Cement Concr. Res. 93 (2017) 71–82, https://doi.org/10.1016/j.cemconres.2016.11.013.
[30] T.M. Chrisp, G. Starrs, W.J. Mccarter, E. Rouchotas, J. Blewett, Temperature-conductivity relationships for concrete: an activation energy approach, J. Mater. Sci. Lett. 20 (2001) 1085–1087.
[31] M. Heikal, M.S. Morsy, I. Aiad, Effect of treatment temperature on the early hydration characteristics of superplasticized silica fume blended cement pastes, Cement Concr. Res. 35 (2005) 680–687, https://doi.org/10.1016/j.cemconres.2004.06.012.
[32] W.J. Weiss, C. Qiao, B. Isgor, J. Olek, Implementing Rapid Durability Measure for Concrete Using Resistivity and Formation Factor, (n.d.) 25.
[33] K.A. Snyder, X. Feng, B.D. Keen, T.O. Mason, Estimating the electrical conductivity of cement paste pore solutions from OH−, K+ and Na+ concentrations, Cement Concr. Res. 33 (2003) 793–798, https://doi.org/10.1016/S0008-8846(02)01068-2.
[34] R. Spragg, C. Villani, K. Snyder, D. Bentz, J.W. Bullard, J. Weiss, Factors that influence electrical resistivity measurements in cementitious systems, Transp. Res. Rec. J. Transp. Res. Board. 2342 (2013) 90–98, https://doi.org/10.3141/2342-11.
[35] H.W. Whittington, J. McCarter, M.C. Forde, The conduction of electricity through concrete, Mag. Concr. Res. 33 (1981) 48–60, https://doi.org/10.1680/macr.1981.33.114.48.
[36] L. Xiao, Z. Li, Early-age hydration of fresh concrete monitored by non-contact electrical resistivity measurement, Cement Concr. Res. 38 (2008) 312–319, https://doi.org/10.1016/j.cemconres.2007.09.027.
[37] X. Wei, L. Xiao, Z. Li, Prediction of standard compressive strength of cement by the electrical resistivity measurement, Construct. Build. Mater. 31 (2012) 341–346, https://doi.org/10.1016/j.conbuildmat.2011.12.111.
[38] A. Lübeck, A.L.G. Gastaldini, D.S. Barin, H.C. Siqueira, Compressive strength and electrical properties of concrete with white Portland cement and blast-furnace slag, Cem. Concr. Compos. 34 (2012) 392–399, https://doi.org/10.1016/j.cemconcomp.2011.11.017.

[39] Q. Gui, M. Qin, K. Li, Gas permeability and electrical conductivity of structural concretes: impact of pore structure and pore saturation, Cement Concr. Res. 89 (2016) 109–119, https://doi.org/10.1016/j.cemconres.2016.08.009.
[40] W. Wilson, F. Georget, K. Scrivener, Unravelling chloride transport/microstructure relationships for blended-cement pastes with the mini-migration method, Cement Concr. Res. 140 (2021), 106264, https://doi.org/10.1016/j.cemconres.2020.106264.
[41] W. Wilson, F. Georget, K. Scrivener, Unravelling chloride transport/microstructure relationships for blended-cement pastes with the mini-migration method, Cement Concr. Res. 140 (2021), 106264, https://doi.org/10.1016/j.cemconres.2020.106264.
[42] S.E. Chidiac, M. Shafikhani, Electrical resistivity model for quantifying concrete chloride diffusion coefficient, Cem. Concr. Compos. 113 (2020), 103707, https://doi.org/10.1016/j.cemconcomp.2020.103707.
[43] K. Scrivener, Advances in understanding cement hydration mechanisms, Cement Concr. Res. (2019) 16.
[44] P.N. Sen, C. Scala, M.H. Cohen, A self-similar model for sedimentary rocks with application to the dielectric constant of fused glass beads, Geophysics 46 (1981) 781–795, https://doi.org/10.1190/1.1441215.
[45] B. Sioulas, J.G. Sanjayan, The coloration phenomenon associated with slag blended cements, Cement Concr. Res. 31 (2001) 313–320, https://doi.org/10.1016/S0008-8846(00)00371-9.
[46] J.D. Rhoades, P.A.C. Raats, R.J. Prather, Effects of liquid-phase electrical conductivity, water content, and surface conductivity on bulk soil electrical conductivity, Soil Sci. Soc. Am. J. 40 (1976) 651–655, https://doi.org/10.2136/sssaj1976.03615995004000050017x.
[47] B. Lothenbach, K. Scrivener, R.D. Hooton, Supplementary cementitious materials, Cement Concr. Res. 41 (2011) 1244–1256, https://doi.org/10.1016/j.cemconres.2010.12.001.
[48] B. Lothenbach, F. Winnefeld, C. Alder, E. Wieland, P. Lunk, Effect of temperature on the pore solution, microstructure and hydration products of Portland cement pastes, Cement Concr. Res. 37 (2007) 483–491, https://doi.org/10.1016/j.cemconres.2006.11.016.
[49] D.M. Kirby, J.J. Biernacki, The effect of water-to-cement ratio on the hydration kinetics of tricalcium silicate cements: testing the two-step hydration hypothesis, Cement Concr. Res. 42 (2012) 1147–1156, https://doi.org/10.1016/j.cemconres.2012.05.009.
[50] W.J. McCarter, G. Starrs, T.M. Chrisp, Immittance spectra for Portland cement/fly ash-based binders during early hydration, Cement Concr. Res. (1999) 11.
[51] J.M. Cruz, I.C. Fita, L. Soriano, J. Payá, M.V. Borrachero, The use of electrical impedance spectroscopy for monitoring the hydration products of Portland cement mortars with high percentage of pozzolans, Cement Concr. Res. 50 (2013) 51–61, https://doi.org/10.1016/j.cemconres.2013.03.019.
[52] R.M. Kowalczyk, A.M. Gajewicz, P.J. McDonald, The mechanism of water–isopropanol exchange in cement pastes evidenced by NMR relaxometry, RSC Adv. 4 (2014) 20709–20715, https://doi.org/10.1039/C4RA00889H.
[53] Z. Zhang, G.W. Scherer, Physical and chemical effects of isopropanol exchange in cement-based materials, Cement Concr. Res. 145 (2021), 106461, https://doi.org/10.1016/j.cemconres.2021.106461.
[54] I. Pane, W. Hansen, Investigation of blended cement hydration by isothermal calorimetry and thermal analysis, Cement Concr. Res. 35 (2005) 1155–1164, https://doi.org/10.1016/j.cemconres.2004.10.027.
[55] B. Lothenbach, G. Le Saout, E. Gallucci, K. Scrivener, Influence of limestone on the hydration of Portland cements, Cement Concr. Res. 38 (2008) 848–860, https://doi.org/10.1016/j.cemconres.2008.01.002.
[56] J.I. Escalante-García, J.H. Sharp, Effect of temperature on the hydration of the main clinker phases in portland cements: part ii, blended cements, Cement Concr. Res. 28 (1998) 1259–1274, https://doi.org/10.1016/S0008-8846(98)00107-0.
[57] L. Lam, Y.L. Wong, C.S. Poon, Degree of hydration and gel/space ratio of high-volume fly ash/cement systems, Cement Concr. Res. 30 (2000) 747–756, https://doi.org/10.1016/S0008-8846(00)00213-1.
[58] J.I. Escalante-Garcia, Nonevaporable water from neat OPC and replacement materials in composite cements hydrated at different temperatures, Cement Concr. Res. 33 (2003) 1883–1888, https://doi.org/10.1016/S0008-8846(03)00208-4.
[59] N. Schwarz, N. Neithalath, Influence of a fine glass powder on cement hydration: comparison to fly ash and modeling the degree of hydration, Cement Concr. Res. 38 (2008) 429–436, https://doi.org/10.1016/j.cemconres.2007.12.001.
[60] F. Avet, R. Snellings, A. Alujas Diaz, M. Ben Haha, K. Scrivener, Development of a new rapid, relevant and reliable (R3) test method to evaluate the pozzolanic reactivity of calcined kaolinitic clays, Cement Concr. Res. 85 (2016) 1–11, https://doi.org/10.1016/j.cemconres.2016.02.015.
[61] Z.-X. Tang, D. Claveau, R. Corcuff, K. Belkacemi, J. Arul, Preparation of nano-CaO using thermal-decomposition method, Mater. Lett. 62 (2008) 2096–2098, https://doi.org/10.1016/j.matlet.2007.11.053.
[62] S. Adu-Amankwah, M. Zajac, C. Stabler, B. Lothenbach, L. Black, Influence of limestone on the hydration of ternary slag cements, Cement Concr. Res. 100 (2017) 96–109, https://doi.org/10.1016/j.cemconres.2017.05.013.
[63] F.W. Locher, Cement: Principles of Production and Use, Verlag Bau+ Technik, 2013.
[64] L.J. Struble, The Influence of Cement Pore Solution on Alkali-Silica Reaction, Ph. D. thesis, Purdue University, 1987.
[65] J. Bockris, Modern Electrochemistry: an Introduction to an Interdisciplinary Area, ume 1, Springer Science & Business Media, 2012.
[66] J. Johnston, The change of the equivalent conductance of ions with the temperature, J. Am. Chem. Soc. 31 (1909) 1010–1020, https://doi.org/10.1021/ja01939a003.
[67] F. Deschner, F. Winnefeld, B. Lothenbach, S. Seufert, P. Schwesig, S. Dittrich, F. Goetz-Neunhoeffer, J. Neubauer, Hydration of Portland cement with high replacement by siliceous fly ash, Cement Concr. Res. 42 (2012) 1389–1400, https://doi.org/10.1016/j.cemconres.2012.06.009.
[68] C. Shi, Effect of mixing proportions of concrete on its electrical conductivity and the rapid chloride permeability test (ASTM C1202 or ASSHTO T277) results, Cement Concr. Res. 34 (2004) 537–545, https://doi.org/10.1016/j.cemconres.2003.09.007.
[69] G.E. Archie, The electrical resistivity log as an aid in determining some reservoir characteristics, Trans. AIME 146 (1942) 54–62, https://doi.org/10.2118/942054-G.
[70] P.J. Tumidajski, A.S. Schumacher, S. Perron, P. Gu, J.J. Beaudoin, On the relationship between porosity and electrical resistivity in cementitious systems, Cement Concr. Res. 26 (1996) 539–544, https://doi.org/10.1016/0008-8846(96)00017-8.
[71] M.K. Moradllo, Relating formation factor of concrete to water absorption, ACI Mater. J. 13 (2018).
[72] J. Zhang, E.A. Weissinger, S. Peethamparan, G.W. Scherer, Early hydration and setting of oil well cement, Cement Concr. Res. 40 (2010) 1023–1033, https://doi.org/10.1016/j.cemconres.2010.03.014.
[73] E.J. Garboczi, Permeability, diffusivity, and microstructural parameters: a critical review, Cement Concr. Res. 20 (1990) 591–601, https://doi.org/10.1016/0008-8846(90)90101-3.
[74] D. Jansen, F. Goetz-Neunhoeffer, C. Stabler, J. Neubauer, A remastered external standard method applied to the quantification of early OPC hydration, Cement Concr. Res. 41 (2011) 602–608, https://doi.org/10.1016/j.cemconres.2011.03.004.
[75] D. Jansen, Ch. Naber, D. Ectors, Z. Lu, X.-M. Kong, F. Goetz-Neunhoeffer, J. Neubauer, The early hydration of OPC investigated by in-situ XRD, heat flow calorimetry, pore water analysis and 1 H NMR: learning about adsorbed ions from a complete mass balance approach, Cement Concr. Res. 109 (2018) 230–242, https://doi.org/10.1016/j.cemconres.2018.04.017.
[76] P.T. Durdziński, M. Ben Haha, S.A. Bernal, N. De Belie, E. Gruyaert, B. Lothenbach, E. Menéndez Méndez, J.L. Provis, A. Schöler, C. Stabler, Z. Tan, Y. Villagrán Zaccardi, A. Vollpracht, F. Winnefeld, M. Zając, K.L. Scrivener, Outcomes of the RILEM round robin on degree of reaction of slag and fly ash in blended cements, Mater. Struct. 50 (2017) 135, https://doi.org/10.1617/s11527-017-1002-1.
[77] E. Nägele, The zeta-potential of cement, Cement Concr. Res. 15 (1985) 453–462.
[78] Z. Giergiczny, Fly ash and slag, Cement Concr. Res. 124 (2019), 105826, https://doi.org/10.1016/j.cemconres.2019.105826.
[79] K.C. Newlands, M. Foss, T. Matchei, J. Skibsted, D.E. Macphee, Early stage dissolution characteristics of aluminosilicate glasses with blast furnace slag- and fly-ash-like compositions, J. Am. Ceram. Soc. 100 (2017) 1941–1955, https://doi.org/10.1111/jace.14716.
[80] J. Skibsted, R. Snellings, Reactivity of supplementary cementitious materials (SCMs) in cement blends, Cement Concr. Res. 124 (2019), 105799, https://doi.org/10.1016/j.cemconres.2019.105799.
[81] D. Lootens, P. Jousset, L. Martinie, N. Roussel, R.J. Flatt, Yield stress during setting of cement pastes from penetration tests, Cement Concr. Res. 39 (2009) 401–408, https://doi.org/10.1016/j.cemconres.2009.01.012.
[82] J.L. Provis, P. Duxson, J.S.J. van Deventer, The role of particle technology in developing sustainable construction materials, Adv. Powder Technol. 21 (2010) 2–7, https://doi.org/10.1016/j.apt.2009.10.006.
[83] Apparent diffusivity model for concrete containing supplementary cementitious materials, ACI Mater. J. 110 (2013), https://doi.org/10.14359/51686338.
[84] K. Stanish, M. Thomas, The use of bulk diffusion tests to establish time-dependent concrete chloride diffusion coefficients, Cement Concr. Res. 33 (2003) 55–62, https://doi.org/10.1016/S0008-8846(02)00925-0.
[85] M.D.A. Thomas, P.B. Bamforth, Modelling chloride diffusion in concrete Effect of fly ash and slag, Cement Concr. Res. (1999) 9.
[86] T. Luping, J. Gulikers, On the mathematics of time-dependent apparent chloride diffusion coefficient in concrete, Cement Concr. Res. 37 (2007) 589–595, https://doi.org/10.1016/j.cemconres.2007.01.006.
[87] J.W. Bullard, M. D'Ambrosia, Z. Grasley, W. Hansen, N. Kidner, D. Lange, P. Lura, T.O. Mason, J. Moon, F. Rajabipour, A Comparison of test methods for early-age behavior of cementitious materials, in: RILEM 2nd Symp, Adv. Concr. Sci. Eng., 2006.
[88] G. Sant, M. Dehadrai, D. Bentz, P. Lura, C.F. Ferraris, J.W. Bullard, J. Weiss, Detecting the fluid-to-solid transition in cement pastes, Concr. Int. 31 (2009) 53–58.
[89] Y. Chen, I. Odler, On the origin of portland cement setting, Cement Concr. Res. 22 (1992) 1130–1140, https://doi.org/10.1016/0008-8846(92)90042-T.
[90] R. Ylmén, U. Jäglid, B.-M. Steenari, I. Panas, Early hydration and setting of Portland cement monitored by IR, SEM and Vicat techniques, Cement Concr. Res. 39 (2009) 433–439, https://doi.org/10.1016/j.cemconres.2009.01.017.
[91] R. Sriravindrarajah, R.N. Swamy, Development of a conductivity probe to monitor setting time and moisture movement in concrete, Cem. Concr. Aggregates 4 (1982) 73–80.
[92] C. Villat, V.X. Tran, N. Pradelle-Plasse, P. Ponthiaux, F. Wenger, B. Grosgogeat, P. Colon, Impedance methodology: a new way to characterize the setting reaction of dental cements, Dent. Mater. 26 (2010) 1127–1132, https://doi.org/10.1016/j.dental.2010.07.013.

[93] İ.B. Topçu, T. Uygunoğlu, İ. Hocaoğlu, Electrical conductivity of setting cement paste with different mineral admixtures, Construct. Build. Mater. 28 (2012) 414–420, https://doi.org/10.1016/j.conbuildmat.2011.08.068.
[94] E.R.A. Jr, G.H. Smith, The significance of particle shape in formation resistivity factor-porosity relationships, J. Petrol. Technol. 7.
[95] J.P. Straley, Critical phenomena in resistor networks, J. Phys. C Solid State Phys. 9 (1976) 783–795, https://doi.org/10.1088/0022-3719/9/5/017.
[96] I. Webman, J. Jortner, M.H. Cohen, Numerical simulation of continuous percolation conductivity, Phys. Rev. B 14 (1976) 4737–4740, https://doi.org/10.1103/PhysRevB.14.4737.
[97] F. Leng, N. Feng, X. Lu, An experimental study on the properties of resistance to diffusion of chloride ions of fly ash and blast furnace slag concrete, Cement Concr. Res. 30 (2000) 989–992, https://doi.org/10.1016/S0008-8846(00)00250-7.
[98] R.A. Meyers, Encyclopedia of Physical Science and Technology, Academic, 2002.
[99] L. Tong, O.E. Gjørv, Chloride diffusivity based on migration testing, Cement Concr. Res. 31 (2001) 973–982, https://doi.org/10.1016/S0008-8846(01)00525-7.
[100] N. Neithalath, J. Jain, Relating rapid chloride transport parameters of concretes to microstructural features extracted from electrical impedance, Cement Concr. Res. 40 (2010) 1041–1051, https://doi.org/10.1016/j.cemconres.2010.02.016.
[101] J. Weiss, K. Snyder, J. Bullard, D. Bentz, Using a saturation function to interpret the electrical properties of partially saturated concrete, J. Mater. Civ. Eng. 25 (2013) 1097–1106, https://doi.org/10.1061/(ASCE)MT.1943-5533.0000549.
[102] T. Luping, J. Gulikers, On the mathematics of time-dependent apparent chloride diffusion coefficient in concrete, Cement Concr. Res. 37 (2007) 589–595.